Review on magnonics with engineered spin textures

Daniela Petti[1,*], Silvia Tacchi[2,*] and Edoardo Albisetti[1,*]

1. *Dipartimento di Fisica, Politecnico di Milano, Italy.*
2. *Istituto Officina del Materiali, Consiglio Nazionale delle Ricerche (CNR-IOM), Italy.*

Email: daniela.petti@polimi.it, tacchi@iom.cnr.it and edoardo.albisetti@polimi.it

Published DOI: https://iopscience.iop.org/article/10.1088/1361-6463/ac6465

Abstract

Spin textures, such as non-uniform domain arrangements, domain walls and skyrmions are naturally occurring structures in magnetic materials. Recently, the unique properties of spin textures such as their reconfigurability, stability and scalability towards nanoscale dimensions, has sparkled the interests towards their use as active elements in spintronic devices. In the framework of magnonics, which aims to use spin waves for carrying and processing information, using spin textures allows to harness an extremely rich phenomenology for designing new functionalities. In this review, we focus on the recent developments on the control and stabilization of engineered spin textures, and their applications in the field of magnonics. First, we introduce the main techniques used for stabilizing the spin textures and controlling their properties. Then we review the recent results on the use of engineered spin textures for guiding, emitting and manipulating spin waves, and report on recent proposals on the realization complex functionalities using integrated spin-texture-based systems, which hint to possible future directions for technological prospects.

1. Introduction

The ability to control the spin texture, i.e. the spatial arrangement of spins, of magnetic materials has fostered the possibility to study in-depth its interaction with particles and quasiparticles, as well as use it as a functional element in devices. In particular, non-uniform spin textures, such as tailored magnetic domains, domain walls, vortices or skyrmions, have attracted remarkable attention due to their stability, scalability towards the nanoscale and reconfigurability with external stimuli such as magnetic fields or currents. Spin textures have therefore become the basis of several proposals for devices across the fields of spintronics, ranging from racetrack memories based on domain walls [1] or skyrmions [2], to magnetic vortex oscillators [3,4].

In the field of magnonics [5–8], which aims to use spin waves (SWs) for information processing, the study and use of spin textures has recently received a considerable boost. This is due to the extremely rich phenomenology involving the combination of SWs and spin textures, and due to the potential of spin textures to provide solutions to some of the outstanding challenges of the field. Among these, the SW confinement and zero-field guidance at the nanoscale, the emission of sub-μm wavelength SWs, and the spatial manipulation of the wavefront shape, phase and SW interference are highly sought after capabilities which are hard to achieve with conventional methodologies.

At the same time, the possibility to effectively study and employ spin textures as functional elements in magnonics goes hand in hand with the ability to stabilize a wide variety of textures, with controlled properties and a high level of complexity.

In this paper, first the methodologies and techniques which allow for controlling the spin texture of magnetic materials are reviewed. Then, the focus is set on describing the recent experimental advances regarding the use of spin textures as functional elements in magnonics. Specifically, the review is divided in the following sections:

Methodologies and techniques for spin-texture engineering. Here, an overview of the experimental techniques which can be employed for controlling the spin texture in magnetic materials are presented. They range from conventional lithography, to the direct irradiation with charged particles, to scanning probe techniques, to exploiting the interaction with suitable substrates and/or coupling effects within the material itself.

Spatial control and SW guidance. In this section, the spin texture is employed as a means to spatially control the SW propagation. The cases of magnetic domains and domain walls (DWs) employed as waveguides for spatially confining and steering SWs is reviewed.

Spin-wave emission. Here, we review the tunable excitation of SWs using nanoscale spin textures as emitters, ranging from vortex cores to magnetic DWs.

Interaction and manipulation of spin waves via spin textures. In this section, the works regarding the manipulation of the SW properties during propagation using spin textures are reviewed. This rich

phenomenology ranges from the control over the amplitude and phase by DWs, to the SW reflection and refraction at domain walls, to the observation of dynamic modes in stripe domains and three-dimensional spin textures.

Complex magnonic devices and systems. Here, the focus lays on experiments and proposals aiming to use spin textures for realizing complex functionalities in devices. Examples are SW devices such as circuits, diodes and logic gates based on domain wall waveguides, electric control of the spin wave propagation, devices exploiting non-linear effects, and devices based on antiferromagnetic spin textures.

Conclusions and outlook. In this final chapter, the conclusions and future perspectives of the field are discussed.

2. Methodology for spin-texture engineering

The capability of controlling and stabilizing spin textures with tailored properties and nanoscale resolution is a fundamental requirement in order to study new phenomena and design and realize new spintronic devices. The patterning of magnetic materials was first proposed for magnetic data storage applications and relied on the use of conventional optical and electron beam lithography. However, given the difficulties in precisely controlling the spin configuration of the materials via the geometry of the pattern and the shape anisotropy, other approaches were developed. For instance, charged particles have been exploited for ion irradiation, i.e. for producing a local change in the material properties affecting the magnetic behaviour. A similar concept was implemented via the scanning probe techniques, which employ different stimuli (e.g., magnetic, thermal, electric…) to modify the magnetic properties of thin films. A different approach is represented instead by exploiting the interaction of the substrate via magnetoelectric and magnetoelastic effects to stabilize different domain configurations.

2.1 Conventional lithography

Conventional micro and nanofabrication is the most widely-used approach to control the magnetic properties of materials. Regarding the stabilization of spin textures, it relies primarily on the use of shape anisotropy to stabilize different domain configurations. In the most common approach, the shaping of the material is obtained by creating suitable photoresist masks via optical and electron-beam lithography (EBL) for the subsequent additive, i.e. deposition and lift off, or subtractive, i.e. etching and stripping, processes. This approach was first exploited in the field of magnetic storage media, where the spin configuration of magnetic nanoparticles was studied in order to achieve single domain structures and to assess the superparamagnetic limit [9]. Figure 1 (c) reports the Magnet Force Microscope image (MFM) 140 nm x 250 nm Co ellipses fabricated via electron-beam lithography, evaporation and lift-off; the white/dark contrast indicates the presence of single domains [10]. More recently, conventional lithography was employed in the fabrication of racetrack memories or logic devices, exploiting the shape of the conduits for controlling the nucleation, pinning and propagation of domain walls [1] and complex spin textures such as skyrmions [11]. Figure 1 (a), (b) shows the MFM images of domain walls pinned in a triangular notch in a Py nanowire. The width and the internal structure of the domain wall can be controlled by the width of the nanowire, since they depend on the magnetostatic field arising from the shape of the structure. In panel (a) the black contrast corresponds to tail-to-tail transverse domain walls or vortices in wires 200 nm (left) and 300 nm (right) wide. In panel (b) the white contrast is given by head-to-head domain walls or vortices; in this case the width of the lithographed structures is 200 nm (left) and 400 (right) nm. In circular nanostructures, the spin configuration of the vortex structures can be tuned by controlling the dimension of the patterned structure [12]. For instance, if the dot thickness is much smaller than the diameter, the magnetization tends to stay in the plane of the sample, while the spins within a small spot in the core of the vortex turns perpendicular to the plane. In panel (d) the MFM image of $Ni_{80}Fe_{20}$ dots 50 nm thick and 1 μm in diameter, fabricated by e-beam lithography, evaporation and lift-off, shows such a spin configuration, where the dark or white spots represent the out of plane spin in the core. It is worth to notice that however, without considering other anisotropies, shape anisotropy alone cannot deterministically set the circularity or the polarity of the vortex, the latest being controllable by an

external magnetic field [13,14]. Panel (e) reports the image from photoemission electron microscopy (PEEM) of an artificial skyrmion stabilized by fabricating an epitaxial Co vortex disk with in-plane magnetization on top of an out-of-plane magnetized Ni film. 30-nm-thick Co circular disks (radius 1 μm) are grown epitaxially on the substrate by using shadow masks. The sketch shown in the figure corresponds to a N=0 configuration of the artificial skyrmion, in which the spin of the central core (Co disk) is parallel to the surrounding spins (Ni films). The configuration can be switched to a N=1 state in which the spins of the core are antiparallel to the surrounding, by applying an out of plane magnetic field.

Finally, among conventional techniques, nanoimprint lithography (NIL) is a low-cost technology, which however assures high throughput and resolution. NIL is based on using a stamp with nanometric features for mechanically imprinting a pattern on suitable resists. After releasing the stamp, a complementary pattern is defined in the resist layer. Then, additive and/or subtractive processes are performed for transferring the resist pattern into the substrate. Figure 1 (f), shows the MFM image (top) of the demagnetized state Co microbars fabricated by NIL. The formation of different spin textures (e.g., vortex, diamond, cross tie..), which are determined by the aspect ratio of the bar, are visible [15]. The simulations and corresponding spin configuration (bottom) are consistent with the experimental data.

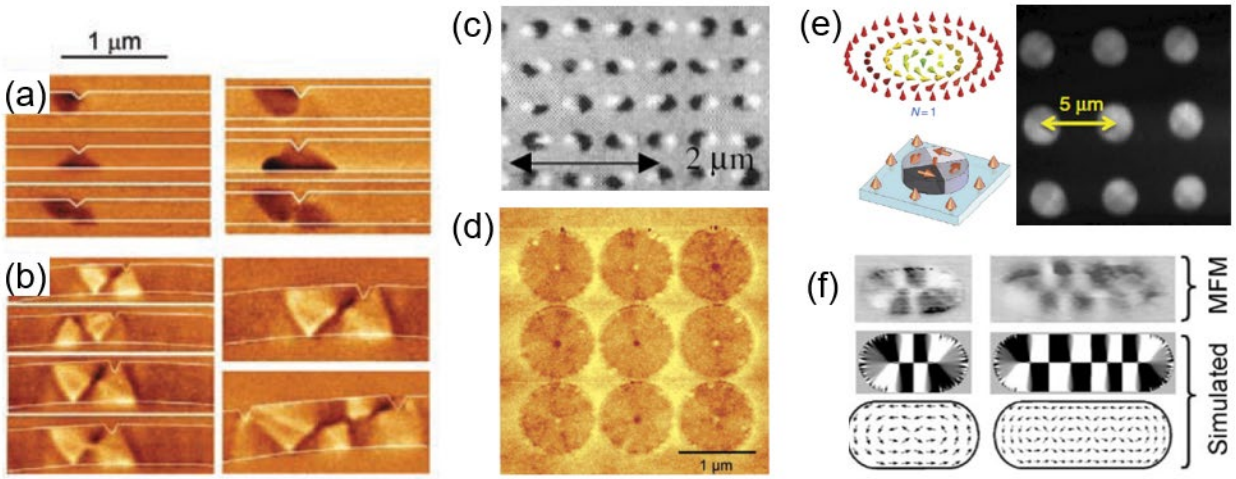

Figure 1. Conventional lithography. (a)-(b) MFM image of Nèel and Vortex domain walls stabilized in 10 nm thick, 200-300 nm wide Permalloy nanowire racetracks fabricated via Electron Beam Lithography [1]. (c) MFM image of 7 nm thick elliptical cobalt dots fabricated via EBL, in a monodomain magnetic state[10]. (d). MFM image of permalloy circuilar dots fabricated via EBL and evaporation, hosting magnetic vortices[12]. (e) Left: spin configuration of a magnetic skyrmion stabilized in a the Co(disk)/Ni(30 Ml)/Cu(001) structure fabricated using a shadow mask. Right: PEEM image of the magnetic configuration within the dots [14]. (f) MFM and simulated multi-vortex state of 35 nm thick, 700 nm wide cobalt nanostructures fabricated with nanoimprint lithography and electrodeposition. [15]

2.2 Charged particles: irradiation and assisted deposition

The direct interaction of charged particles, such as ions and electrons, with the magnetic material is exploited in milling and irradiation. Ion milling, commonly via Ar+ ions, is used in combination with lithography to etch photoresist-masked films. Ion milling can be also performed via focused ion beam, which uses Ga+ ions and allows the direct-writing of nanostructures down to 10-15 nm resolution. As already mentioned, in this case the structuring of the magnetic materials leads to a control of the magnetic properties through shape anisotropy [16].

A different approach is represented by ion irradiation. In this case, charged particles (e.g. Ar, Ga, N, and He), penetrating the magnetic films and losing energy along their trajectory, can locally modify the morphology, crystalline structure, grain size, chemical composition, interface, strain, vacancy and defects density of the system, depending on the ionic type, energy and dose employed [17]. Consequently, a direct tailoring of the magnetic anisotropies, coercive fields, magnetic moments and exchange interactions is possible. Irradiation uses beam energies in the 0.3-150 keV range and doses from $2*10^{-14}$ to $5*10^{-16}$ ions cm^{-2}, while at higher doses etching becomes not negligible. As in the case of milling, the spatial resolution is achieved by using a resist mask [18,19] or by using a focused ion beam [20–23]. In Figure 2 (a), low energy He+ ions are used in combination with a resist mask to pattern 100 nm-wide magnetic domains. In this case, the mechanism exploited is a reduction of a Co_3O_4/Pd paramagnetic superlattice to a Co/Pd ferromagnetic superlattice with strong perpendicular magnetic anisotropy [19]. Ion irradiation is also employed in combination with exchange bias systems [24]. In such systems, the exchange interaction at the interface of the two layers gives rise to an unidirectional anisotropy in the ferromagnetic film, which phenomenologically corresponds to a shift of the hysteresis loop by a quantity called exchange bias field. If the exchange bias is strong enough, the magnetization of the system at remanence is pinned in the direction of the exchange bias field. In this framework, in [25], the authors use ion irradiation for spatially controlling both the direction and strength of the unidirectional anisotropy, and creating a tailored magnetic domain wall charge landscape.

Irradiation has been also demonstrated with electron beams; in Figure 2 (b), P. Genoni and co-authors used micro-focused low energy (50-100 eV) e-beam to change the magnetic anisotropy of ultrathin hcp Co films from in-plane to perpendicular to the plane [26].In this case, by irradiating the film in CO ambient, atomic carbon is accumulated on the surface of the film and then converted in a single graphitic layer with a subsequential annealing at 170°C in UHV. The presence of the graphitic carbon changes the magnetic anisotropy of the Co films and also stabilizes a sizable Dzyaloshinskii−Moriya interaction (DMI), as the chemomagnetic pattern shows the formation of chiral Néel domain walls (Figure 2 (b), right panel). Electron beam irradiation was also used for patterning skyrmions in exchange biased systems composed by a ferromagnet and antiferromagnet, with perpendicular magnetic anisotropy [27] (see Figure 2 (c)). Here, a focused electron beam is used to locally stabilize single domain configurations. The mechanism underneath the patterning is a combination of thermal effects and electron excitations which changes the magnetic order of the antiferromagnet and stabilizes a uniform exchange bias direction. Due to the presence of DMI, by reducing the size of the patterned domain, a single skyrmion with diameter of 150

nm is stabilized; in Figure 2 (c), right panel an artificial skyrmion lattice with honeycomb configuration is demonstrated.

As a final remark, charged particles were also used to assist the chemical vapour deposition of material (focused ion beam or focused electron beam induced deposition) in three dimensional nanostructures. The precursor molecules in gaseous forms are injected onto the substrate surface and a focused beam of electrons/ions is scanned on the substrate, creating a deposit with the same shape formed by the scanning beam. Different precursors are available for deposition of different magnetic materials, such as $Co_2(CO)_8$, $Co(CO)_3NO$, $Fe(CO)_5$, $Fe(C_5H_5)_2$, $HFeCo_3(CO)_{12}$ and $Ni(C_5H_4CH_3)_2$ [28]. As in conventional lithography, the main mechanism to control the formation of spin textures is via shape anisotropy and the main geometries employed are nanowires with different aspect ratio. In Figure 2 (d), an example of Co nanostripes growth by FEBID with a field-emission scanning electron microscope and a $Co_2(CO)_8$ as gas precursor on Si is reported [29]. The different domain configurations and spin textures as a function of the aspect ratio of the nanostructures are visible in the magnetic force microscope (MFM) image in Figure 2 (d), right panel.

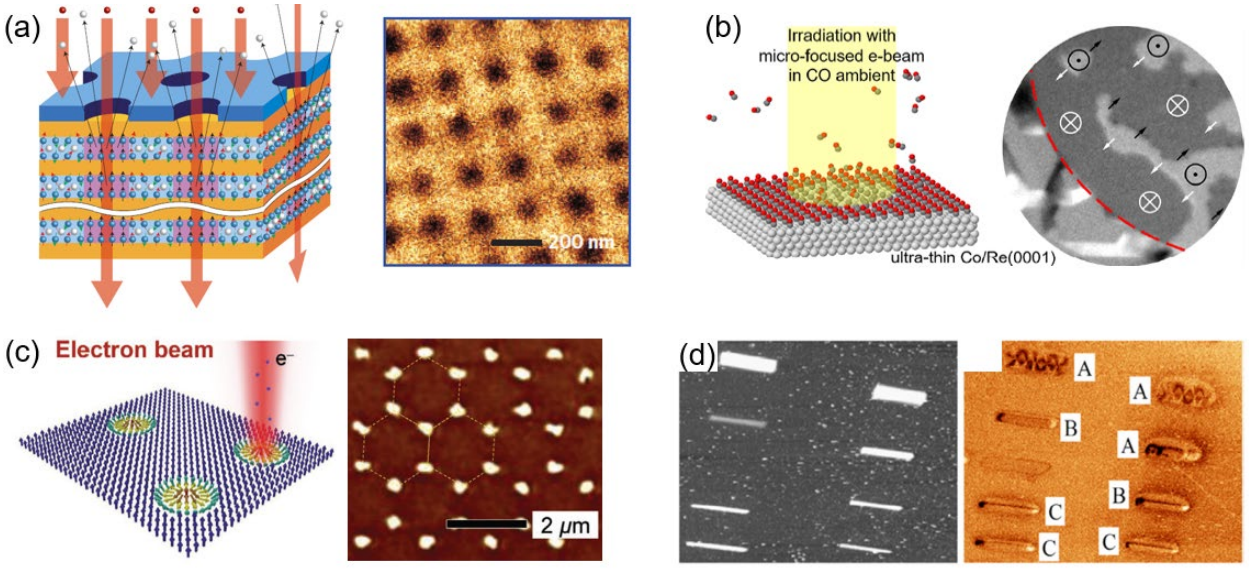

Figure 2. Patterning with charged particles. (a) Left: non-destructive patterning of the magnetic properties of a magnetic multilayer via low-energy proton exposure. Right: MFM image of 100-nm wide dot patterns with perpendicular magnetic anisotropy [19]. (b) Left: patterning ultrathin Co films via electron-beam assisted carbon lithography. Right: PEEM magnetic image of the patterned region [26]. (c) Left: Magnetic skyrmions are written in an exchange bias magnetic multilayer via focused E-beam irradiation. Right: MFM image of a honeycomb skyrmion lattice patterned via E-beam irradiation [27]. (d) Topography (left) and MFM image (right) of Focused Electron-Beam Induced Deposited nanowires [29]

2.3 Scanning Probe Lithography

Scanning Probe Lithography (SPL) [30] is based on the use of a nanometric probe to produce local surface modifications. A variety of SPL approaches was developed due to the different interactions the tip can have with the substrate, which depend mainly on the nature of the tip (e.g. thermal, magnetic, conductive..) and on the type of surface. Another factor distinguishing the different techniques is the nature of the signal used to control the probe vertical position during the scan (e.g. via tunneling current, atomic force, evanescent electromagnetic wave).

Among SPL techniques, thermal Scanning Probe Lithography (tSPL) [31] employs an atomic force microscope or dedicated thermal lithography tool and relies on the nanoscale confinement of the heat produced by a heatable Si probe. Such thermal probes were originally developed by IBM for data storage applications [32], and consist of specially designed cantilevers integrating a resistive micro-heater above the tip. By flowing an electric current, the heater temperature can be precisely controlled from RT up to ~1200 °C. Different thermally-mediated effects can be exploited for lithography, e.g. thermally assisted nanoindentation or degradation, thermochemical modifications of surfaces or deprotection of functional groups in polymers.

Thermally assisted magnetic Scanning Probe Lithography (tam-SPL) [33] is based on scanning the heated probe on the surface of a magnetic system with an applied external magnetic field. In particular, in Figure 3 (a), the patterning mechanism is sketched in case of an exchanged bias multilayer with in plane anisotropy.

During the patterning, a localized field cooling is performed only in the region where the tip is scanned, which is able to set a new exchange bias and hence a novel unidirectional anisotropy. As a consequence, different domains with different magnetization directions at remanence can be patterned. Note that the patterning prepared using this technique is purely magnetic, is tunable, reconfigurable and resilient to external magnetic perturbations. Different spin textures can be patterned by choosing the geometry of the pattern and the external magnetic field. In Figure 3 (b), the MFM image of different domains written in a CoFeB/IrMn systems is shown, while Figure 3 (c) shows the MFM image and related micromagnetic simulations of a magnetic vortex with controlled topology, stabilized within a Nèel wall [34]. The patterning of spin textures in exchange biased synthetic antiferromagnets [35] has been also demonstrated.

By using the tip of a magnetic force microscope it is possible to exploit the magnetic interaction of the stray field arising from the tip with the magnetic substrate. Two examples of the use of this technique are illustated in Figure 3 (d), (e) and Figure (f), (g). In the first case [36], the combination of the stray field of the probe and of an external applied filed is used to selectively switch the spin of single domain NiFe nanoislands (300 nm long, 80 nm wide) in an array. The nanoislands array is design in order to obtain an artificial spin structure in which it is possible to obtain via MFM multiple longrange orderings of a magnetic charge ice lattice at room temperature. By applying different writing protocols, it is possible to write different charge ice configurations in a reconfigurable way; for example, in Figure 3 (e), a type II_2 order is written onto a freshly erased area previously patterned in a type III_3 configuration. In the work of J. C.

Gartside et al. [37] a high momentum MFM tip induces a vortex in a nanowire which is eventually moved by the tip perpendicular to the nanostructure long axis, without the need of an external field (Figure 3 (f)). The vortex forms a pair of 180° asymmetric domain walls and once the tip crossed the wire, the most unstable moves towards one end of the wire unwinding and giving rise to a collinear state. This process favours the switching of the magnetization to the opposite direction with respect to the initial one. This approach was used to selectively write nanowires 1 μm long and 75 nm wide, arranged in a Kagome artificial spin ice (Figure 3 (g)), giving rise to different spin configurations corresponding to various artificial spin ice macrostates.

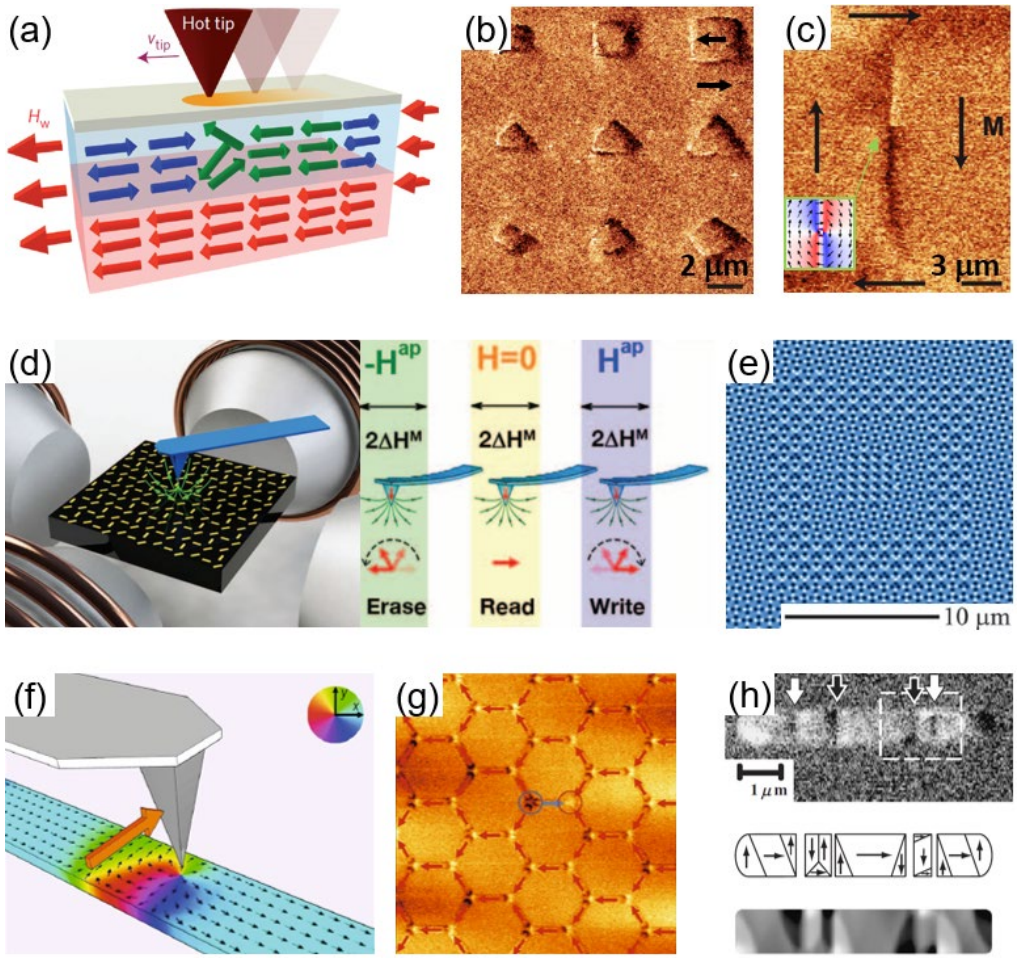

Figure 3. Patterning with Scanning Probes. (a)-(c) Patterning 2D domains, 1D domain walls and 0D topological solitons via thermally-assisted magnetic scanning probe lithography (tam-SPL). (a) A heated AFM tip is swept in presence of an external magnetic field for locally re-setting the exchange bias and directly writing spin textures. (b) MFM image of arbitrary-shaped magnetic domains written via tam-SPL in a CoFeB/IrMn bilayer [33] (c) A patterned vortex Bloch line within a Nèel wall. Inset shows the corresponding micromagnetic simulation. [34] (d)-(e) An MFM tip in combination with an external field is used for deterministically writing the ground state of artificial spin ice structures fabricated via EBL. [36] (f)-(g) An MFM tip is used for writing the ground state of artificial spin ice by inducing transient topological magnetic defects [37]. (h) Nano-oxidation with a conductive AFM tip is used for writing Co oxide NWs in a Co structure and controlling the domain structure [38].

A last example of SPL with a conductive probe is reported in Figure 3 (h) [38]. When a negative voltage is applied to the tip, an anodic oxidation process takes place, due to the electrochemical reaction between the metallic thin film and water in air. The sample consists in Co-based single-domain rectangular nanostructures of 5.1 μm length and 0.8 μm width fabricated on top of Pt contacts, which assure the flow of current from the tip to the substrate. The top figure in the panel shows an MFM image of the Co rectangle with the oxide nanowires fabricated across, while, in the bottom panel, the calculated magnetic configuration and the corresponding micromagnetic simulations are reported. Via nano-oxidation is therefore possible to divide the sample in different magnetic domains and stabilize different domain configuration by controlling the position and geometry of the pattern.

2.4 Interaction with the substrate

A different approach which does not require lithographic steps on the magnetic material is the stabilization of the spin textures via interaction with the substrate. Depending on the nature of the system, a variety of phenomena can be exploited: morphology, strain, magneto-electric coupling, multiferroicity, coupling with surface acoustic waves, are few examples.

In Figure 4 (a), the nanopatterning of the films is obtained through use of nanoporous alumina membranes. It consists of an array of ordered nanodomes, whose curvature is able to induce magnetic anisotropy and an effective Dzyaloshinskii−Moriya interaction (DMI) in the magnetic overlayer. The emergence of these interactions leads to magnetochiral effects and topologically induces magnetization patterning. Figure 4 (a), left panel, shows the MFM image from an array of 100 nm nanodomes on which a Pt/Co/Ta multilayer has been deposited. The image demonstrates the stabilization of skyrmions at the zero field that are arranged following the topography of the nanostructure [39].

Strain engineering was widely used in perovskite films displaying ferromagnetic or antiferromagnetic character. By choosing a suitable substrate or buffer layer, it is possible to modify the strain of thin films from compressive to tensile and, due to the strong interplay among crystal field, charge, orbitals and magnetism, to tune the magnetic properties. In Figure 4 (b), strain engineering was applied to $BiFeO_3$ thin films. The image shows an in-plane PiezoForce Microscope (PFM) phase image of $BiFeO_3$ films grown on $SrTiO_3$ and the correspondent Nitrogen Vacancy (NV) magnetic microscopy image of the spin configuration [40]. It is found that for compressive and low tensile strain, the spin cycloids propagate in a single direction within a ferroelectric domain, i.e. there is a correspondence between the two type of domains. For high tensile strain, the periodicity connected to the ferroelectric domains is lost and the spin cycloidal order appears to be strongly destabilized.

Finally, the coupling between ferroelectric and magnetic domains was exploited also in multiferroic heterostructures consisting of a ferroelectric substrate ($BaTiO_3$) and a thin magnetic film (CoFe) [41]. In this case, the magnetic configuration is an exact copy of the ferroelectric domain structure in the as-grown state, as sketched in Figure 4 (c), where a stripe ferroelectric (FE) domain induces a stripe magnetic pattern in the ferromagnet (FM). The arrows in FE indicate the orientation of the in-plane ferroelectric polarization, while those in the FM corresponds to the magnetic easy axis. By applying an out-of-plane electric field, the FE domains change and the strip pattern rotates by 45°. At the same time, the magnetic

spin texture is modified as a superposition of two patterns: one is the exact copy of the rotated domains and one is the as-grown patterns. On the other hand, the rotation of the FE polarization from in-plane to out-of-plane does not significantly alter the domain configuration of the FE films. This is due to lattice symmetries and to the coupling mechanism among the domains, which is based on strain.

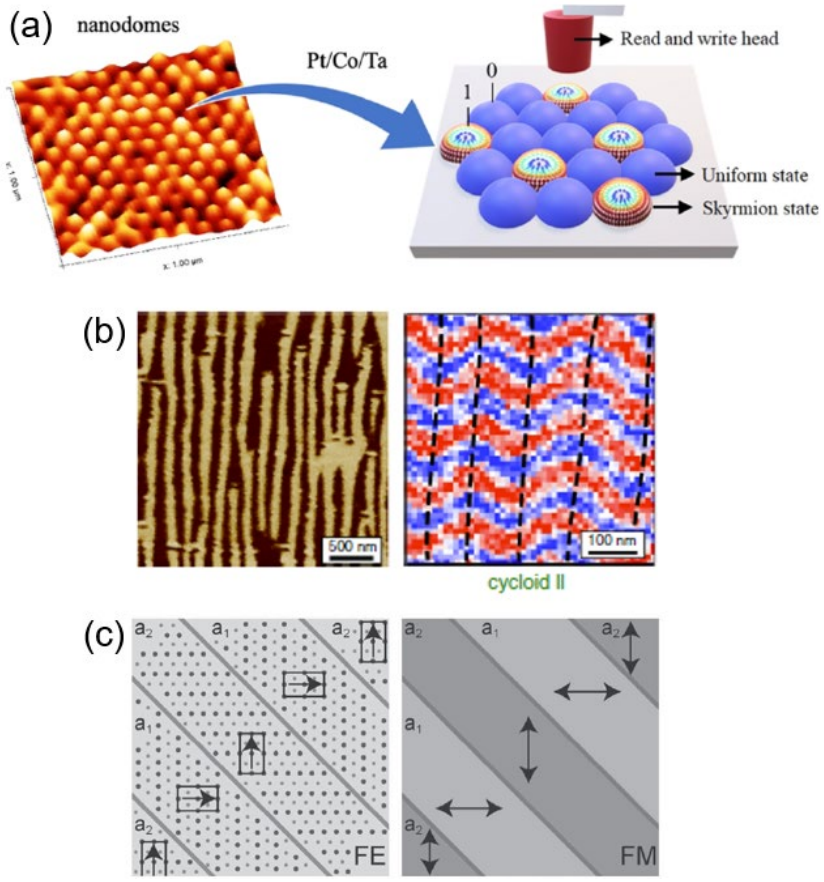

Figure 4. Spin textures stabilized exploiting the interaction with the substrate. (a) Zero-field Skyrmion crystals are stabilized naturally on arrays of self-assembled nanodomes [39] (b) Ferroelectric domains in STO/$BiFeO_3$ measured via PFM (left) and corresponding non-collinear antiferromagnetic spin textures (right) measured via NV-center magnetometry [40]. (c) Schematic of the ferroelectric domain structure (left), imprinted in the ferromagnetic domain structure (right) in BiFeO3 / CoFe bilayers [41].

3. Spatial control and spin-wave guidance

In the field of magnonics, the capability of efficiently channeling and steering of spin waves is essential for the implementation of SWs circuits and devices. Usually controlling and guiding spin-wave propagation are realized exploiting geometrically patterned waveguides. In such kind of structure propagation along curved waveguide has been demonstrated experimentally using external fields [42,43] or arrays of nanomagnets [44]. However, these approaches don't provide the flexibility needed for reprogrammable devices and require the application of magnetic fields, implying a high energy consumption. In addition, such structures are hardly scalable towards nanoscale dimensions due to the limitations of the lithographic techniques and crosstalk between densely packed devices. In this section we review recent works which experimentally demonstrated that spin textures, such as tailored domain structures and magnetic DWs, are a very promising route to realize efficient SWs waveguides.

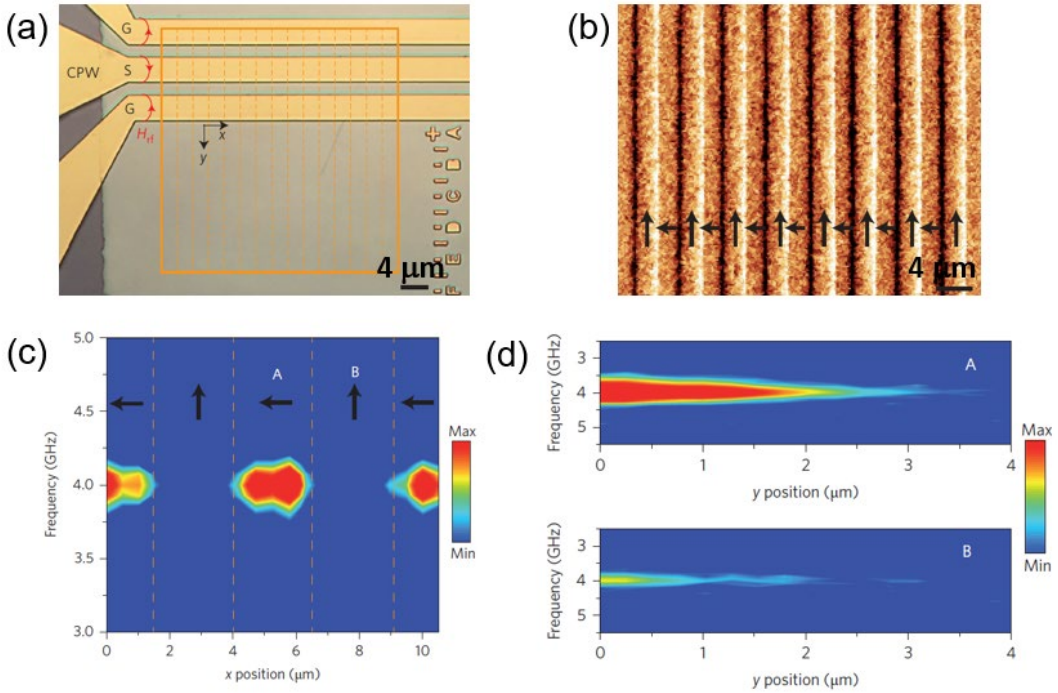

Figure 5. Spatial control of SW excitation and propagation using nanopatterned magnetic domains. (a) Optical image of the sample. A coplanar waveguide (CPW) run by RF current is used for exciting the SW is the continuous CoFeB/IrMn film. (b) 2.5 μm wide magnetic domain tracks written via tam-SPL. The black arrows indicate the magnetization direction. (c)-(d) Line maps of the SW intensity acquired via μ-BLS along the CPW arm (x direction), and perpendicular to it (y-direction). A sizeable SW intensity is measured only within the domains where the magnetization is parallel to the CPW, i.e. in the Damon-Eshbach configuration.

In [33], E. Albisetti et al. demonstrated the use of a tailored magnetic domain structure as a magnonic waveguide. The authors used tam-SPL technique to prepare 2.5-μm-wide tracks with alternating 0° and 90° oriented remanent magnetization (Figure 5 (b)), in an exchange bias system consisting of a Ru(2nm)/IrMn(7nm)/CoFeB(5nm) multilayer deposited on a Si substrate. A coplanar waveguide, oriented perpendicular to the direction of the tracks, was used for SWs excitation (Figure 5 (a)), while SWs

propagation was mapped by micro-focused Brillouin Light Scattering (μ-BLS) measurements. Figure 5 (c) reports the SWs intensity measured at remanence along the CPW arms, performing a μ-BLS linear scan just outside the CPW itself. One can see that SWs are efficiently excited only in type A tracks, where the local magnetization is parallel to the CPW, whereas in type B tracks, where the local magnetization is perpendicular to the CPW, the efficiency of the SWs excitation is strongly reduced. This finding is explained taking into account that in this CPW geometry, the SWs excitation efficiency mainly results from the coupling between the in-plane component of the microwave field and the corresponding component of the dynamical magnetization, associated with the SWs. Therefore, in type A (B) the coupling efficiency is high (low) due to the parallel (perpendicular) alignment of the in-plane component of the micro-wave field and the corresponding component of the dynamic magnetization. In addition, as it can be observed in the BLS maps measured as a function of distance from the CPW (Figure 5 (d)), in the centre of two adjacent tracks, SWs attenuate rapidly in the type B track, whereas in the type A track they are able to propagate for several microns, covering a propagation distance similar to those observed in lithographically patterned waveguides. This behavior can be ascribed to the anisotropy of SWs propagation. In particular, for perpendicular alignment of the SWs wavevector and local magnetization (corresponding the magnetostatic surface wave configuration), the group velocity of the spin waves is much larger than for parallel alignment (corresponding the magnetostatic backward volume configuration).

Nanoscale DWs in thin films were proposed as magnonic nano-waveguides to both channel and steer propagating SWs. After the seminal study of Winter [45], predicting SWs channeling in Bloch type DWs, SWs propagation has been theoretically investigated in recent works. Garcia-Sanchez et al. [46] predicted theoretically and by means of micromagnetic simulations the SWs channeling in DWs, separating two uniformly magnetized up and down domains in thin films having a large perpendicular magnetic anisotropy (PMA). They find that SWs can propagate both in Bloch and Néel type DWs, which acts as a local potential well for SWs. For Néel-type DWs a marked nonreciprocal channeling is observed, arising from the DMI. Moreover, the authors show that SWs can be guided in curved DWs with a 90° bend without loss of coherence. More recently, Y. Henry and coauthors [47] investigated, by using micromagnetic simulations, SWs propagation inside Bloch DWs formed between up and down domains, occurring in stripe domains (SDs) patterns. In thin ferromagnetic films, SDs develop as stripes with the perpendicular component of the magnetization pointing alternately up and down with respect to the film surface, due to the competition between the short-range exchange coupling, the long-range magnetostatic interaction, and the perpendicular magnetic anisotropy (PMA). In particular, the formation of SDs was observed in a variety of structures suca as thin magnetic films [48–51], having large PMA, and in systems with moderate or low PMA, but above a critical thickness [52,53].

The authors find the SWs propagation in a single DW is strongly nonreciprocal due to the dynamic dipolar interactions. Moreover, for arrays of parallel DWs in a SDs pattern, the sequence of up/down and down/up walls with opposite nonreciprocities leads to the formation of a complex SW band structure.

The experimental evidence for SWs propagation in narrow magnonic waveguides based on DWs was given by K. Wagner et al. [54] combining μ-BLS measurements and micromagnetic simulations. The investigated

sample consists of a $Ni_{81}Fe_{19}$ bar where a Landau-like domain pattern was stabilized with a 180 degrees Néel wall in the center separating two domains in-plane magnetized in opposite directions. A microwave antenna is positioned at the beginning of the $Ni_{81}Fe_{19}$ bar for SWs excitation (Figure 6 (b)) As it can be seen in Figure 6 (a), the authors observe a SW mode having a frequency of 0.5 GHz which is localized in the position of the DW and propagating away from the antenna. The propagative character of the SWs is confirmed by micromagnetic simulations showing a positive dispersion relation of SWs localized in the DW. From the analysis of the BLS detected signal across the DWs width, the authors find that the width of the SWs nanochannel created by the DW texture is below 100 nm in agreement with micromagnetic simulations indicating a DW width of about 40 nm. Finally, they find that the position of the domain wall can be controlled applying an external magnetic fields along the long axis of the waveguide. Changing the polarity of the field, the growth of either the left or the right domain is favored, inducing a shift of the DWs position. μ-BLS measurements, reported in Figure 6 (c), show that the detected SWs mode is shifted over a distance of several microns, together with the DW, by the applied field indicating a novel method to achieve a reconfigurable control of SWs propagation.

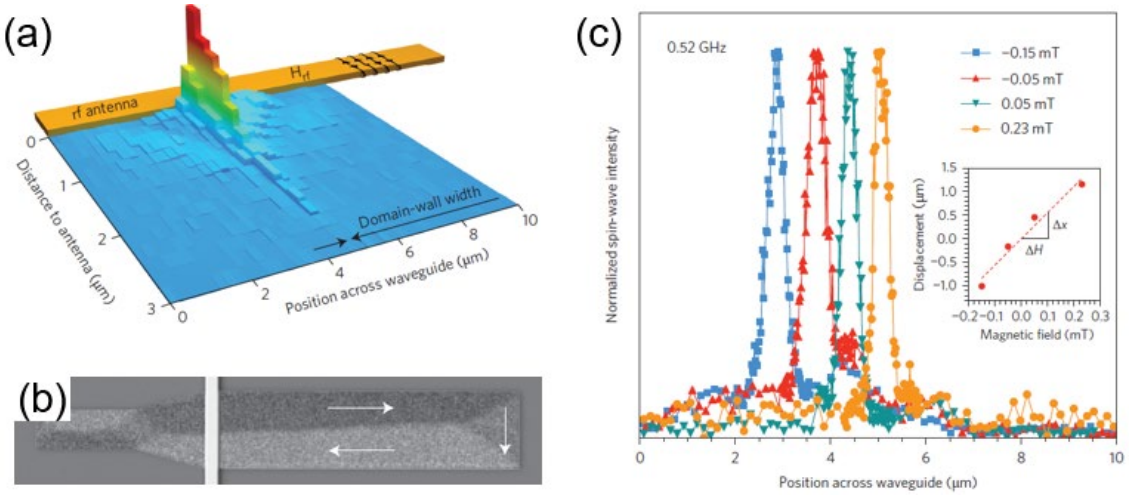

Figure 6. Channeling spin waves with magnetic domain walls. (a) 2D map of the SW intensity measured via μ-BLS outside the RF antenna used for excitation. SWs are detected only in correspondence of the domain wall. (b) Kerr microscopy image of the Landau domain pattern. (c) SW intensity as a function of the external magnetic field. The SW peak is shifted as the domain wall is displaced by the external field. [54]

Subsequently, E. Albisetti et al. [55] experimentally proved the channeling and steering of propagating SWs in reconfigurable nano-magnonic waveguides, based on DWs. Figure 7 (a) reports a schematic picture of the experiments. Spin textures were patterned in an exchange bias ferromagnet/antiferromagnet system, consisting of a $Co_{40}Fe_{40}B_{20}$ (20 nm)/$Ir_{22}Mn_{78}$ (10 nm)/Ru(2 nm) multilayer by using tam-SPL. The latter allowed stabilizing arbitrary shaped 180° Néel DWs by patterning two magnetic domains with antiparallel remanent magnetization (Figure 7 (b)). SWs were excited by means of a microstrip antenna, while time resolved scanning transmission X-ray microscopy (TR-STXM) measurements were exploited to study SWs propagation.

The SW channeling in DWs of different shapes is observed by the authors. Figure 7 (d) reports the snapshots of SWs travelling along a curved path, at remanence, with a frequency of 1.11 GHz, where a SW propagation distance of about 2 μm from the antenna is visible. The propagating character of the SW mode is confirmed by the temporal evolution of the phase of the SWs as observed in the snapshots. The spatial map of the SW amplitude (Figure 7 (c)) indicates that the mode is confined within the DW, with a lateral extension (full width at half maximum) of 115 nm.

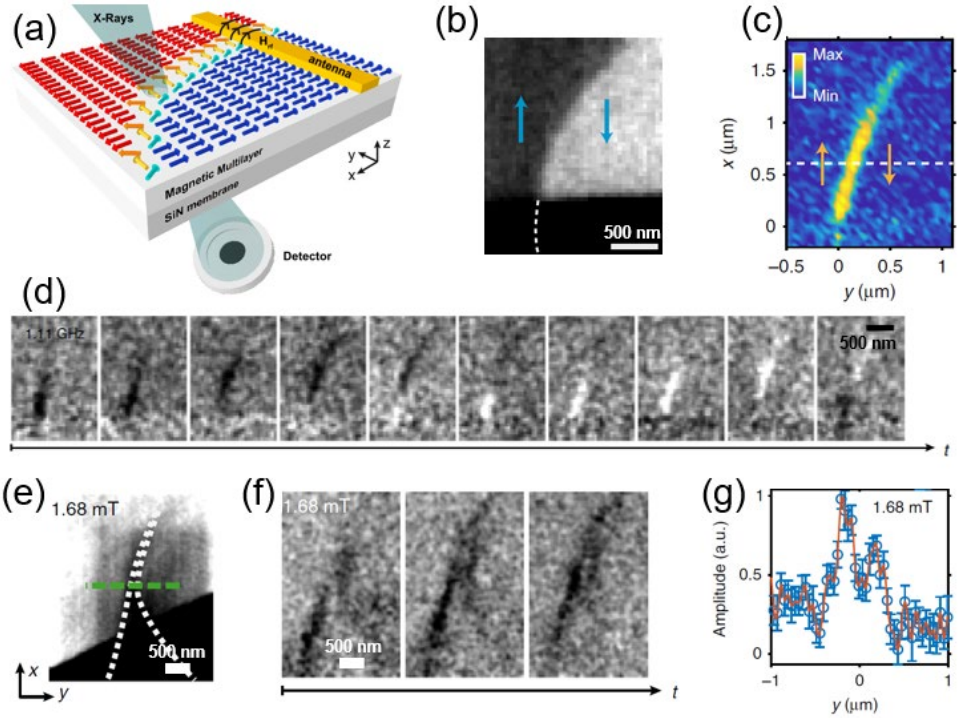

Figure 7. Nanoscale SW circuits based on spin textures. (a) Sketch of a domain wall written via tam-SPL. A stripline run by RF current is used for SW excitation. Time-resolved Scanning X-Ray Microscopy with in-plane sensitivity is used for measuring the magnetic configuration and spin-wave propagation. (b)-(c) Static STXM image of a curved Nèel wall (b) and corresponding 2D map of the SW amplitude showing SW confinement and guidance by the domain wall (c). (d) Frames from a time-resolved STXM video showing the propagating character of the Winter SW modes. (e)-(g) Static magnetic image of two domain walls (dotted white lines) with a common apex. (f) Time-resolved frames of SWs propagating within the two walls and spatially superimposing at the apex. (g) Line profile (green line in (e)) of the SW amplitude, showing spatial superposition of the two modes. [55]

Moreover, tunable spatial superposition and interference of guided SW modes propagating in two converging waveguides is also experimental demonstrated. Figure 7 (e) shows the STXM images of a spin texture comprising two DWs whose separation can be controlled applying a small static magnetic field along the −x-direction. The STXM snapshots for an excitation frequency of 1.28 GHz, and the amplitude of the sinusoidal fit along the horizontal profiles of Figure 7 (e) are reported in Figure 7 (f) and Figure 7 (g), respectively, for a 1.68 mT external magnetic field. The two peaks, with full width at half maximum of about 200 nm, correspond to the two guided modes. When an external magnetic field of 2 mT is applied,

the two modes are spatially separated and do not overlap. On reducing the field down to 1.68 mT, the two modes approach and partially overlap, with a peak-to-peak distance of 340 nm. These findings experimentally proved a fundamental building block of SWs circuitry, paving the way to exploit engineered spin textures as building blocks of SWs based computing devices.

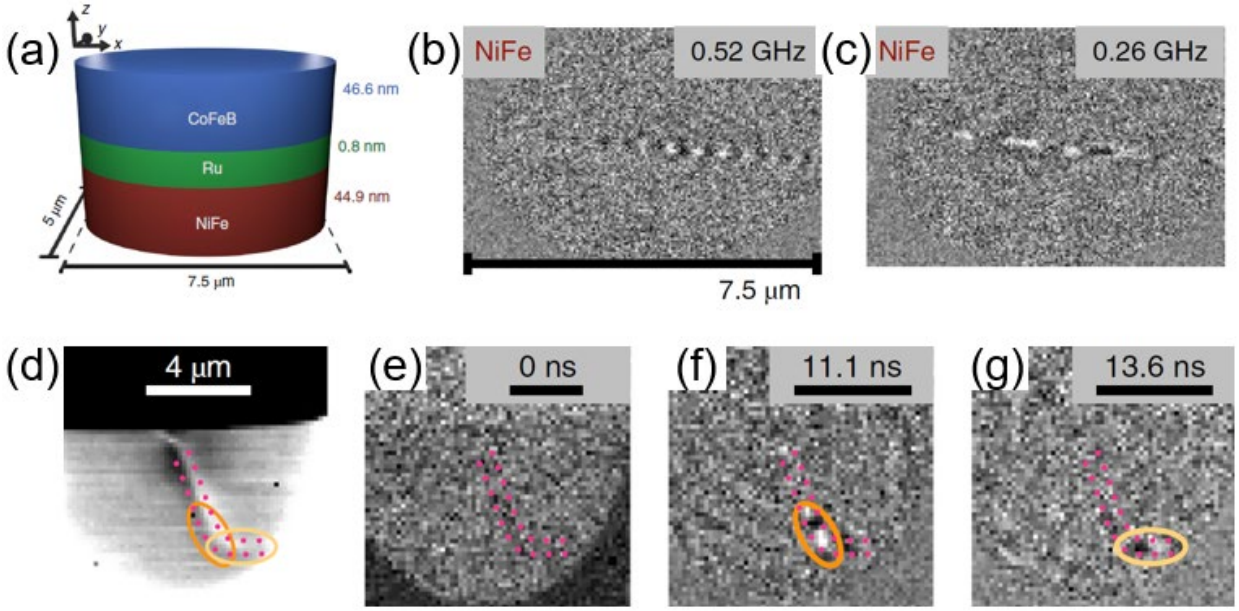

Figure 8. Guiding short-wavelength SWs with domain walls in a synthetic antiferromagnet. (a) Synthetic antiferromagnet elliptical sample structure. The CoFeB and NiFe layers are coupled antiferromagnetically. (b)-(c) Time-resolved STXM frames of SWs at 0.52 GHz (b) and 0.26 GHz (c) emitted by the central vortex and propagating within the domain wall. (d) Static STXM image of a corner-shaped domain wall. (e)-(g) Time-resolved STXM frames of a SW packet travelling within the DW and «turning the corner». [56]

The SWs propagation along straight and curved 180° DWs was also observed using TR-STXM by Sluka et al. in [56]. The investigated sample consists of an elliptical element with lateral sizes of several micrometres, patterned in a synthetic ferrimagnetic (SFi) $Ni_{81}Fe_{19}$(44.9nm)/Ru(0.8nm)/$Co_{40}Fe_{40}B_{20}$(46.6nm) multilayers. At remanence, the magnetic ground-state configuration of this system consists in a pair of vortices, with opposite vorticity due to the antiferromagnetic interlayer exchange coupling. However, the CoFeB in-plane uniaxial anisotropy causes a marked distortion of the vortex magnetization distribution in both magnetic layers, resulting in the stabilization of two homogeneously in-plane magnetized domains with opposite magnetizations in each layer (Figure 8 (a)). These domains are separated by a narrow 180° domain wall which contains the vortex cores and spans along the long axis of the ellipse. Micromagnetic simulations indicate that the DW formed in the sample is a mixture of Néel and Bloch types of DW. As it will be described in more detail in the next paragraph, when the straight DW is excited by an alternating magnetic field at a frequency larger than about 1 GHz, the authors observe SWs emission in the domains. On the contrary, for a lower excitation frequency, SWs emission is no longer observed in the domains, while SWs propagation inside the DW is visible (Figure 8 (b), (c)). This behavior is explained by taking into account that the SWs

dispersion relation of the SFi system is characterized by a frequency gap of about 0.5 GHz, while SWs confined in the DWs are characterized by an almost linear dispersion with an almost zero gap. Therefore, domains cannot support SWs, having a frequency smaller than about 0.5 GHz, which can instead propagate inside the DW. Moreover, they find that SWs are also able to propagate in the same kind of mixed Néel- and Bloch- type DW, having a curved shape. Figure 8 (e)-(g) reports TR-STXM snapshots, taken at different times instants after the excitation field pulse, showing that the SWs packet can travel around the DW corner (Figure 8 (d)) retaining a detectable magnitude.

4. Tunable Spin-wave emission

One of the requirements for using SWs in advanced nanosized magnonic devices is the excitation of SWs with nanoscale wavelengths. However, the limitations of lithographic techniques make challenging to excite propagating SW, having a wavelength lower than 100 nm, using conventional methods based on the spatial localization of RF magnetic fields generated by inductive antennas. In order to overcome these issues, magnetic nanostructures [57,58] in combination with antennas, or the use of spin-transfer torque nano-oscillators [59,60] have been proposed as possible solutions.

Recently, another approach has attracted considerable attention. It has been experimentally demonstrated that the limits of the methods traditionally used for the SWs excitation can be overcame by exploiting the dynamics of nanoscale spin textures such as magnetic vortex cores and domains walls. In the following we present recent experimental works showing the exploitation of these structures as tunable sources to generate SWs having nanoscale wavelengths and to manipulate their propagation properties.

4.1 Tunable Spin-Wave Emission from Vortex Cores

Coherent emission of short-wavelength propagating SWs by the driven gyration of magnetic vortex cores was first observed by S. Wintz et al. in a SFi system formed by a square element, having a lateral size of 4 μm and patterned in a Co(47.8nm)/Ru(0.8nm)/$Ni_{81}Fe_{19}$(42.8nm) trilayer [61]. At remanence the ground state of this structure consists of a pair of stacked magnetic vortices with an in-plane flux-closure of the magnetization and the central cores oriented perpendicular to the film plane (Figure 9 (a)). Due to the antiferromagnetic interlayer coupling, the vortices have opposite in-plane circulations, while the core polarities are parallel due to dipolar coupling. The authors used an in-plane oscillating magnetic field to excite the gyration of the vortex cores, and TR-STXM measurements to image SW emission and propagation. They observed the emission of high-amplitude SWs, which propagate radially from the vortex cores towards the edges of the sample. In addition, the SWs wavelengths is found to be linearly tuned without any external magnetic field by changing the driving frequency reaching a minimum value $\lambda = 125 \pm 10$ nm at f = 4 GHz (Figure 9 (b)-(d)).

Similar experimental investigation was subsequently performed by G. Dieterle et al. for a magnetic vortex naturally formed in a $Ni_{81}Fe_{19}$ circular disk having a diameter of 3 μm and a thickness of 80 nm. [62]. The authors observe a SW radial emission by the driven rotational dynamics of the vortex core also in a single ferromagnetic layer, demonstrating the universality of the phenomenon of the SW emission from magnetic vortex cores. Moreover, in the single layer, SW emission is observed to occur at substantially higher frequencies with respect to the SFi system, and the ultra-short wavelength regime (sub-100 nm) can be attained for an excitation frequency of about 10 GHz.

More recently, S. Mayr et al. experimentally demonstrated, by using of TR-STXM measurements, that the SW emission pattern of a magnetic vortex core can be manipulated by the application of an in-plane static magnetic field [63]. In particular, they studied SW generation from magnetic vortex cores stabilized in disk structures having a diameter of 3 μm and patterned by electron beam lithography in both a SFi system

consisting of a Co(48nm)/Ru(0.8nm)/$Ni_{81}Fe_{19}$(45nm) trilayer and a single Py film 100 nm thick. When a static in-plane magnetic field is applied to the samples, the vortex cores move from the center towards the edge of the disk, expanding the region where the magnetization is aligned parallel to the applied field in order to minimize Zeeman energy. In the SFi structure, the antiferromagnetically coupled cores are observed to simultaneously move in the two layers expanding the region in the Co layer (NiFe layer) where the magnetization is aligned parallel (anti-parallel) to the applied field, due to the lower magnetic moment per unit area of NiFe. Applying a radiofrequency excitation the displaced vortex cores are observed to emit propagating SWs (Figure 9 (a)-(d)). In the SFi sample, the vortex cores maintain a radial SW emission pattern, when they move from the center towards the edge the disk, on increasing the intensity of the static magnetic field.

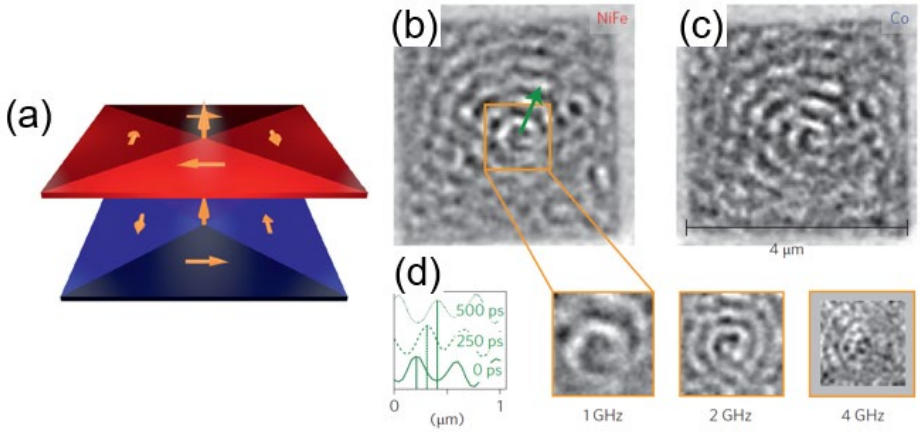

Figure 9. SW emission by vortex cores. (a) Square-shaped synthetic antiferromagnet sample structure. A vortex core is stabilized in the center due to the shape anisotropy. The circularities are opposite in the Co 48 nm and NiFe 43 nm layers. (b)-(c) Time-resolved STXM frame with out-of-plane sensitivity of SWs at 1 GHz emitted by the core and propagating within the domain in the NiFe (b) and Co (c) layer. (d) Left: spatial profile of the SWs along the green line in panel (b). Right: Time-resolved STXM frames showing the wavelength tunability of the SW emission at 1 GHz, 2 GHz and 4 GHz. [61]

In the single Py sample, instead, a modification of the emission pattern is observed on changing the intensity of the static magnetic field. When a moderate field is applied, the vortex core undergoes a small displacement from the center of the disk and maintains a radial spin-wave emission. On the contrary, for higher magnetic fields, the vortex core moves near the edge of the disk and expands following the disk curvature resembling a 180° Bloch domain wall. This expansion changes the vortex core from a zero-dimensional (0D) to a one-dimensional (1D) SW source, leading to the emission of rather planar waves propagating away from the core in both directions perpendicularly to the axis of expansion (Figure 9 (e), (f)). Moreover, a focusing effect is observed towards the center of the disk due to the non-fully planar waves emitted from the curved core. Micromagnetic simulations for the Py sample confirm that the shape and the expansion of the vortex core can be controlled by the intensity of the static magnetic field, affecting the SW emission pattern and the extent of the focusing effect. Finally, the authors observe that the SW wavelength is almost unaffected by the external field for both the circular and the directional emission, since the external magnetic field is compensated by the internal magnetostatic field.

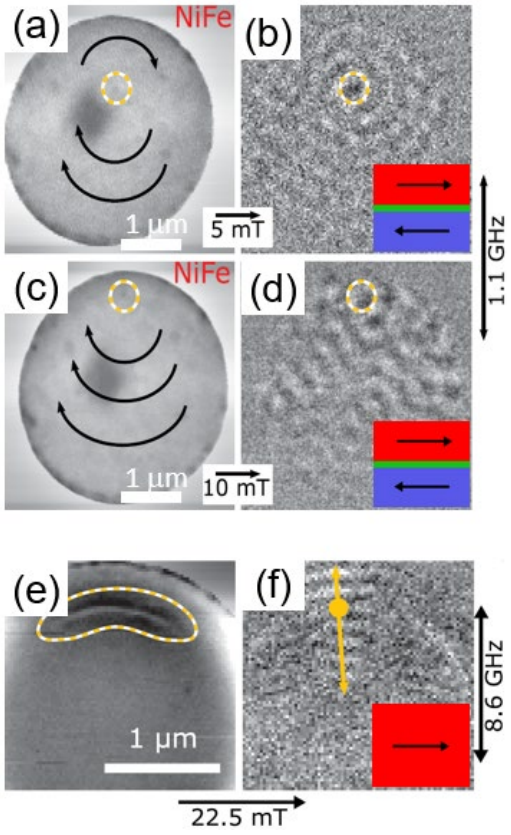

Figure 10. SW emission by vortex cores as a function of the external field. (a)-(d) Time-resolved STXM images with out-of-plane sensitivity showing the location of the vortex core in a synthetic antiferromagnet for H = 5 mT (a) and H = 10 mT (c), and the corresponding propagating SWs emitted at 1.1 GHz by the structure (b) and (d). (e)-(f) Time-resolved STXM images with out-of-plane sensitivity of the magnetic configuration of a single FM layer (e) and corresponding SWs (f) emitted at 8.6 GHz. [63]

4.2 SWs emission from magnetic domain walls

The possibility to generate propagating SWs having short wavelength by the excitation of a DW was first theoretically predicted by micromagnetic simulations by S. J. Hermsdoerfer et al. [64].

In this work the authors investigated the behavior of a pinned DW stabilized in a NiFe layer and excited by an oscillating magnetic field. They find that the applied magnetic field causes an oscillation of the DW itself at the same frequency of the external field. When a steady-state oscillation is reached the DW is observed to emit propagating SWs having a double frequency and a wavelength of about 130nm. In addition, they point out that the SWs emission and properties depend on the oscillation of the out-of-plane component of the dynamical magnetization.

More recently SWs emission from pinned 90 degrees DWs stabilized in a ferromagnetic-ferroelectric bilayer consisting of a strain-coupled CoFe film on $BaTiO_3$ substrate has been demonstrated by

micromagnetic simulations. [65,66] In such a system, DWs are observed emit in the continuous ferromagnetic layer SWs having the same frequency of the excitation current and a wavelength ranging from micrometer length scale to about 100 nm. Very interestingly, in [65] B. Van de Wiele et al. found the properties of the generated SWs can be engineered by patterning of the ferromagnetic film, showing that the effect of the confinement allows an efficient SWs emission at frequencies up to 100 GHz and wavelengths down to 20 nm.

The experimental demonstration of SWs emission by the DWs oscillation has been provided by R. B. Holländer and coworkers [67]. In this work, the authors investigate SWs generation from DWs stabilized in elongated stripes patterned in a $Co_{40}Fe_{40}B_{20}$ film and driven by a microwave field (Figure 11 (a)), using time-resolved magneto-optical Kerr effect (TR-MOKE) measurements. Using micromagnetic simulations, they show that this system can emit SWs having wavelength smaller than 300 nm. However, in the experiments they observe only SWs with micrometer wavelength due to the limited spatial resolution of TR-MOKE technique. Figure 11 (b), (c) show the MOKE image of the domain structure used for SW emission, and a snapshot of the TR-MOKE measurements of propagating SWs emitted by the central wall, respectively.

Lately, investigation of short-wavelength SWs has been performed by means of TR-STXM which allows to reach sub-100 nm spatial and sub-nanosecond temporal resolutions. V. Sluka et al. [56] used TR-STXM measurements to study SWs generation from a straight domain wall stabilized in an elliptical element, patterned in a SFi made of a $Ni_{81}Fe_{19}$(44.9nm)/Ru(0.8nm)/$Co_{40}Fe_{40}B_{20}$(46.6nm) multilayers (Figure 11 (d)). As it was already outlined in the previous paragraph, the magnetic ground-state configuration of the system at remanence results in two homogeneously in-plane magnetized domains with opposite magnetizations in each layer, separated by a mixed Bloch-Neel 180° DW.

When the straight domain wall is excited by an alternating magnetic field, SWs with wavefronts parallel to the domain are observed to propagate away from the domain wall towards the edge of the ellipse, as it can be seen in Figure 11 (e). Emitted SWs are found to have a wavelength between 420 nm and 130 nm, with excitation frequencies ranging from 0.7 GHz to 3 GHz. In addition, the authors observe that the excited SWs can propagate over several microns, spanning multiples of their nanoscale wavelengths, and showing a propagation distance larger than that of SWs generated by the driven gyration of magnetic vortex in a similar SFi trilayer. This difference can be explained taking into account that, in addition to the Gilbert damping, radial SWs emitted from a vortex core suffer an amplitude reduction proportional to the inverse square root of the distance from the source.

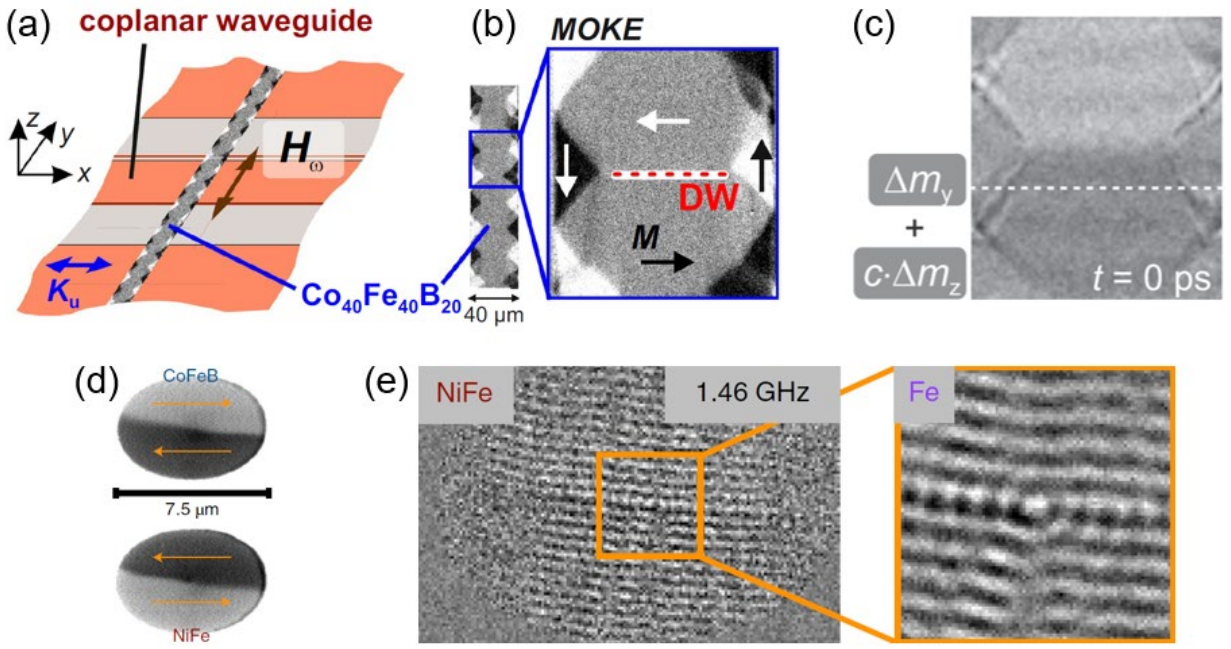

Figure 11. SW emission by domain walls. (a)-(c) Sketch of the sample (a) consisting of a 120 nm thick CoFeB stripe with unaxial anisotropy perpendicular to the stripe length. A coplanar waveguide is used for SW excitation at 9 GHz. Kerr microscopy image (b) of the magnetic configuration and time-resolved Kerr microscopy images of SWs emitted by the wall [67]. (d)-(f) SWs emitted by straight domain wall in a synthetic antiferromagnet, set in oscillation by an RF magnetic field. The sample (d) consists in an elliptical CoFeB / Ru / NiFe trilayer where a straight domain wall is stabilized. The SWs emission at 1.46 GHz and propagation from the wall is visualized via time-resolved STXM imaging. [56]

4.3 Optically-inspired magnonics with engineered spin textures.

Recently, the generation of coherent spatially engineered spin waves wavefronts was demonstrated in a nanoscale optically inspired spin-wave platform [35]. In an exchange biased synthetic antiferromagnet (sy-AF) composed by IrMn/CoFeB/Ru/CoFeB (see Figure 12 (a)) different spin textures are patterned by tam-SPL, by writing magnetic domains with controlled exchange bias and magnetization direction in the two ferromagnetic layers. A radio-frequency (RF) magnetic field generated by a stripline couples with the written spin textures, which are set in oscillation, emitting in turn spin waves which propagate within the domains (Figure 12 (b)). Depending on the spin texture dimensionality and geometry, wavefronts with different shape can be generated: planar wavefronts are emitted by straight domain walls, radial wavefronts from vortices, and concave/convex wavefronts from extended curved domain walls. This is due to the peculiar dispersion of spin waves in SAF [68], presenting a strong non-reciprocal propagation and a low anisotropic dispersion of the short-wavelength branch in a wide angular range. Figure 12 (c), (d) show TR-STXM snapshots, where the white/black contrast corresponds to the oscillation of the out-

of-plane component of the magnetization associated to the propagation of the SWs. In Figure 12 (c) the curved wall emits converging SWs with a short wavelength of 330 nm; in the focal point, the wavefronts change form concave to convex and the width of the beam is in good agreement with the theoretical value arising from a description analogue to diffractive optics. In Figure 12 (d), two magnonic nanoantennas, a straight domain wall and a vortex, emit simultaneously planar and radial wavefronts, giving rise to an interference pattern. Destructive interference fringes correspond to low-intensity, gray regions, while constructive interference is visible as high intensity black/white regions.

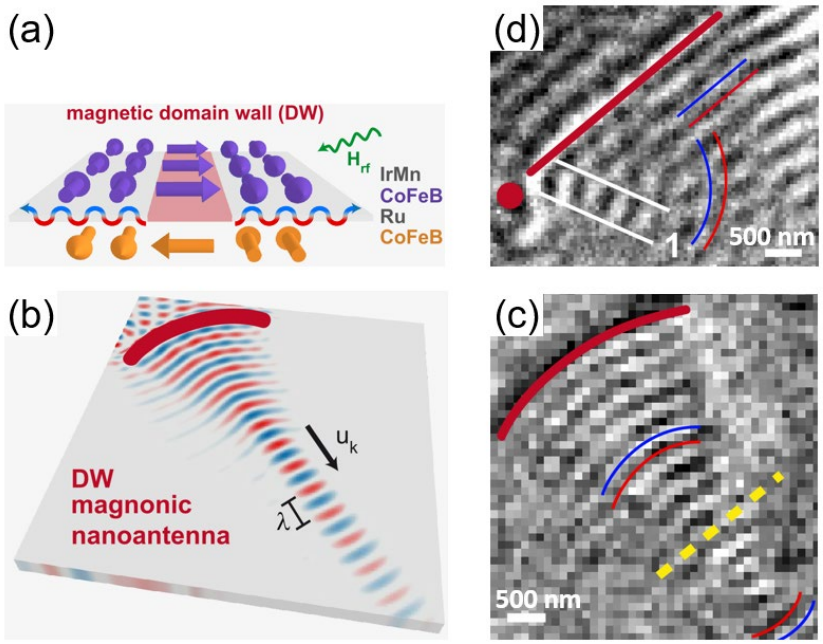

Figure 12. Optically-inspired magnonics with domain-wall nanoantennas. (a) Cross section of the spin configuration of a domain wall in a synthetic antiferromagnet. (b) Micromagnetic simulations of a focused SW beam emitted by a curved domain-wall nanoantenna (red line). (c) Time-resolved STXM image with out-of-plane sensitivity corresponding to the simulations of panel (b). Curved SW wavefronts, marked by the thin red and blue lines are emitted by the wall and are focused in correspondence of the yellow dotted line. (d) Time-resolved STXM image of SW interference by planar wavefronts emitted by a straight wall (magenta line) and radial wavefronts emitted by a vortex (magenta dot). [35]

5. Interaction and manipulation of spin waves

One of the main challenges for the development of efficient SW devices is to control and manipulate SWs propagation. In particular, for advanced SW logic devices based on SW interference, such as SW-interferometers and logic gates, controlling the SW phase is a fundamental requirement. In the last years several different approaches were proposed, including the exploitation of magnetic fields, electric current, elastic strainand artificial magnonic crystals (MCs), artificial structures with a periodic modulation of the magnetic properties. In this context, the manipulation of SWs propagation via magnetic spin textures have been recently suggested as a promising alternative. Analytical calculations [69]and micromagnetic simulations [70] predicted that SWs propagating through a Bloch-type DW are not reflected and only acquire phase shift. On the contrary, it was theoretically [71–74] showed that SWs travelling through Neel-type DWs not only experience a phase shift, but also change their amplitude. In addition, it was demonstrated analytically and by means of micromagnetic simulations, that Neel-type DWs having different chirality, induced by interfacial DMI, causes a different phase change for SWs propagating through them. [75]]. Here we review recent experimental investigations, where magnetic spin textures, as single DW, arrays of SDs, as well as skyrmions were used to manipulate the SW propagation properties.

The first experimental demonstration of SWs reflection from Neel domain walls was given by P. Pirro et. al. [76]. In this work the authors investigate the interaction of SWs, excited by a microwave antenna, with a Landau domain state, consisting of four magnetic domains separated by 90 degrees Neel DWs, stabilized in a square-shaped $Co_2Mn_{0.6}Fe_{0.4}Si$ microstructures (Figure 13 (a)). Using μ-BLS measurements they show that SWs are strongly reflected by Neel DWs for a wide frequency range. Figure 13 (b) show the BLS intensity along the yellow profile in the inset image, showing a sharp decrease in the SW intensity passing across the wall, for a wide frequency range. The non-exponential decay of SWs from the antenna to the vortex core is brought by the authors as a strong indication that SWs are indeed reflected by the walls.

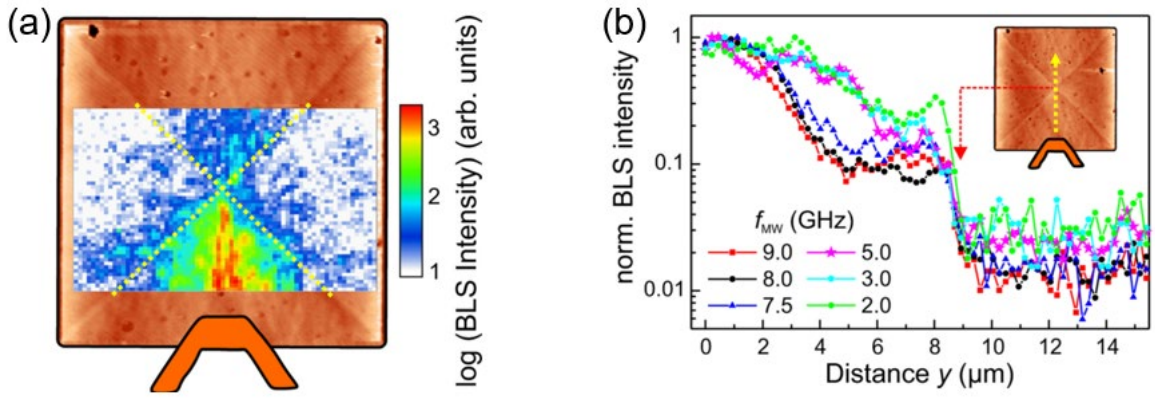

Figure 13. Interaction of SWs with Nèel walls in a Landau configuration. (a) MFM image of the Landau structure in a square-shaped, 20 mm-long edge, 30 nm thick $Co_2Mn_{0.6}Fe_{0.4}Si$ film. Superimposed: sketch of the antenna used for SW excitation at 4.5 GHz, and SW intensity map acquired via μ-BLS. (b) Line profile of the SW intensity along the yellow line in the inset, at different excitation frequencies. A marked decrease of the SW intensity after the wall is observed. [76]

After this pioneering work, very recent studies experimentally proved that changes of the SWs amplitude and the phase as well as of their propagation direction can be induced via interaction with DWs.

The SWs propagation across a 180° Neel-type DW, instead, was investigated by O. Wojewoda et al. [77] A symmetric 180° Neel DW with a circular Bloch line (vortex) in the middle was stabilized in a waveguide patterned in a $Fe_{78}Ni_{22}$ film grown on a Cu (001) single crystal substrate (Figure 14 (a)-(c)). In order to have a stable DW at remanence and allow SW propagation in DE configuration, the waveguide was prepared with the long axis perpendicular to the easy direction of the $Fe_{78}Ni_{22}$ film. Propagation of SWs, excited by a strip line antenna placed on top of the waveguide (Figure 14 (a)), was studied by means of μ-BLS. The SWs transmission across the DW is found to be affected by the presence of the circular Bloch line and to depend on the SW frequency. In the first regime, observed at a frequency of 7.15 GHz, the SW propagation is suppressed near the circular Bloch line and two SWs beams are formed (Figure 14 (d)). On the contrary, in the second regime at 9 GHz, the SWs propagate in a single central beam through the circular Bloch line (Figure 14 (e)). Moreover, phase-resolved μ-BLS measurements show that for both the regimes SWs undergo a phase shift of about 0.5-0.6π upon transmission through the DW, as it can be seen in Figure 14 (f), (g).

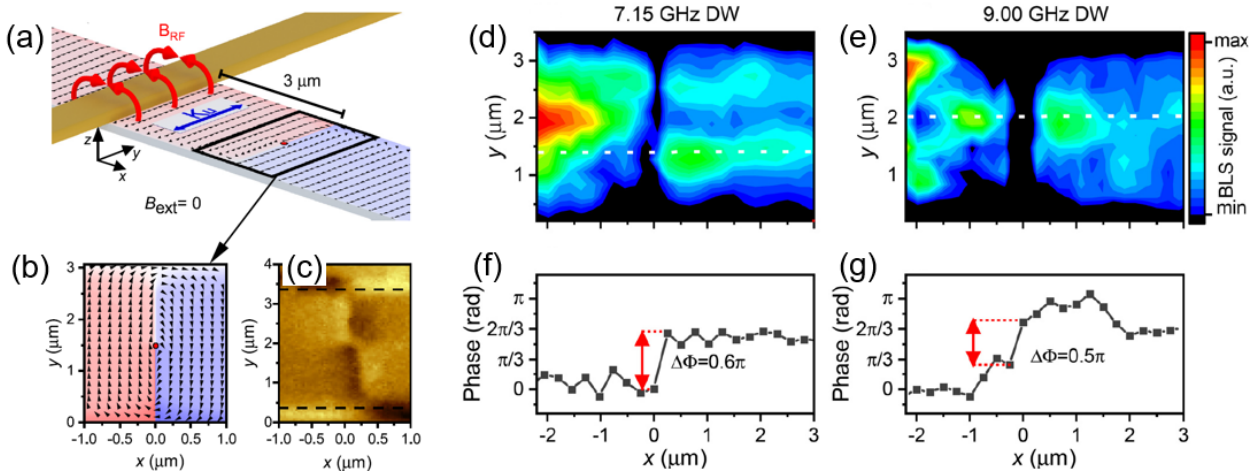

Figure 14. Propagation of SWs through a Nèel wall. (a) Sample sketch, consisting of a 16 nm thick fcc $Fe_{78}Ni_{22}$ stripe with uniaxial anisotropy along the short edge. (b) Micromagnetic simulations and MFM image (c) of the domain structure, showing a Nèel wall hosting a vortex. (d)-(e) μ-BLS map of the SW intensity in the vicinity of the wall for a 7.15 GHz (d) and 9.00 GHz (e) excitation frequency. (f)-(g) SW phase evolution across the wall showing a phase shift of approximately 0.5π across the wall. [77]

Hämäläinen et al., [78] demonstrated that SW transmission across 90° Néel-type DWs can be manipulated on changing the DW texture. They investigated a CoFeB film having a thickness of 50 nm coupled to a ferroelectric $BaTiO_3$ substrate (Figure 15 (a)) characterized by regular ferroelectric stripe domains. Strain transfer and inverse magnetostriction induces in the CoFeB layer the imprinting of magnetic stripe domains, with the anisotropy axis rotated by 90° with respect to each other. By changing the direction of the in-plane saturation field, reconfigurable 90° Néel type DWs at the boundaries of the magnetic stripes

domains can be prepared at remanence. In particular, narrow head-to-tail DWs, having a width of about 50 nm, shown in Figure 15 (b), or broad head-to-head/tail-to-tail DWs, having a width of about 1.6 μm, can be reprogrammed. Using μ-BLS, the authors imaged the propagation of SWs, excited by a stripline antenna, across a domain wall. As it can be seen in Figure 15 (a-c), SWs are found to propagate through broad 90° head-to-head or tail-to-tail DWs, maintaining their amplitude, over a broad frequency range. On the contrary SWs propagation through narrow 90° head-to-tail domain walls is observed to be strongly suppressed. Micromagnetic simulations confirmed such experimental results showing that SWs are resonantly reflected by the head-to-tail domain walls.

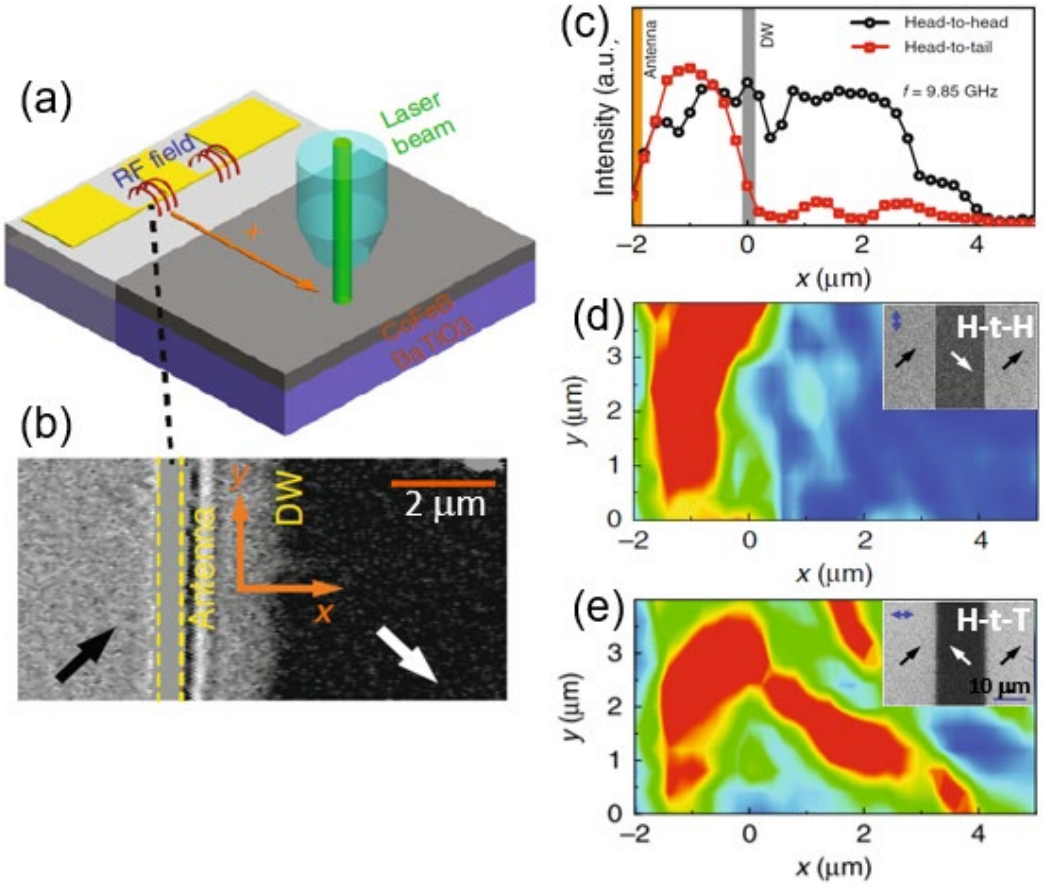

Figure 15. Control of SW transmission with a programmable domain wall. (a) The sample consists of a 50 nm-thick CoFeB film on $BaTiO_3$. An RF antenna is used for exciting SWs and μ-BLS is used for the SW detection. (b) Kerr microscopy image showing the pinned head-to-tail domain wall. (c) Line profile of the SW intensity as a function of the distance from the antenna. The SW intensity at 9.85 GHz is maintained across the DW in the head-to-head configuration, while sharply drops in the head-to-tail configuration. (d)-(e) BLS intensity map in the head-to-head (d) and head-to-tail (e) configuration. [78]

Eventually, T. Hioki et al. [79] experimentally proved that a Neel-type 90° DW is able to induce SWs refraction and reflection. The investigated sample consist of a DW formed at remanence in a $Bi_{0.7}Lu_{2.3}Fe_{4.2}Ga_{0.8}O_{12}$ (LuIG) film and pinned by the crystallographic defects in the sample (Figure 16 (a)).

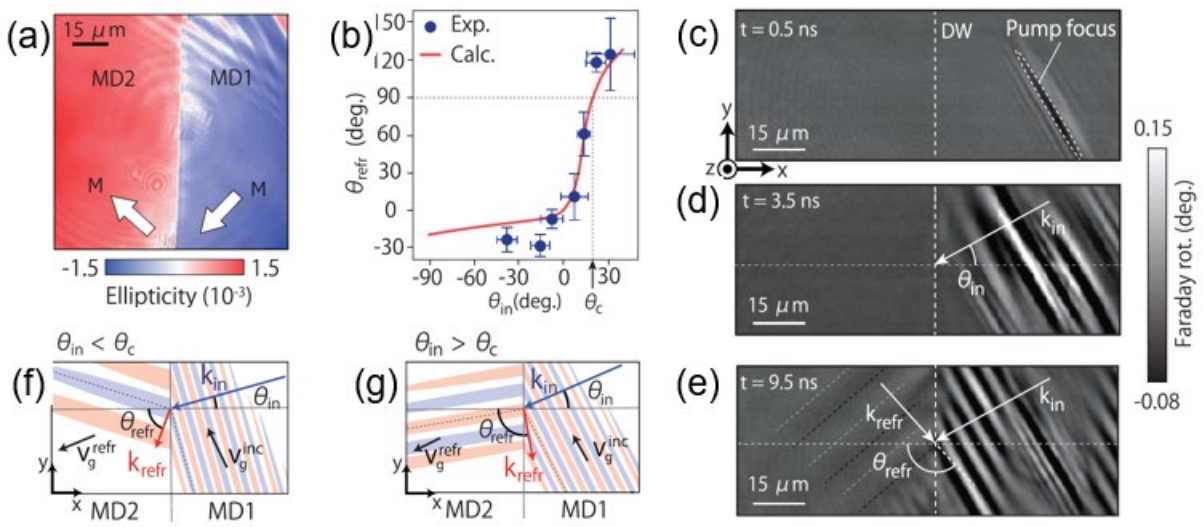

Figure 16. Refraction and reflection of SWs propagating across a 90° domain wall. (a) Static magneto-optical image showing the in-plane component of the magnetization. (b) Experimental and calculated refracted angle as a function of the angle of incidence. (c)-(e) Time-resolved magneto-optical image at different pump-probe delays. The incident and wavevector k_{in} is marked by arrows. (f)-(g) Schematic of incident and refracted SWs in case of $q_{in}<q_c$ (f) and $q_{in}>q_c$ (g). [79]

Planar propagating SWs were generated in the domain MD1 by illumination of a pump beam, while SWs propagation was investigated as a function of the incidence angle θ_{inc} of the excited SWs by using time resolved scanning Kerr microscopy. When $\theta_{inc}>0$ the refraction angle θ_{refr} rapidly increases on increasing θ_{inc}, while θ_{refr} shows a slow variation for $\theta_{inc}<0$. (Figure 16 (b)) Very interestingly when $\theta_{inc}>20.4$ degrees, θ_{ref} assumes values larger than 90°, indicating that SWs undergo negative refraction, as it can be seen in the magneto-optical images Figure 16 (c)-(e), in a similar way to the refraction between two media having refraction indices of opposite signs. The authors demonstrate that the relation between refraction and incident angles can be modeled taking into account the conservation of wavevector component k_y along the DW, and in particular that the negative SWs refraction originates from the anisotropy of the SWs dispersion relation. This effect is illustrated in Figure (f), (g). For $\theta_{inc}< \theta_{ref}$ refracted SWs have negative k_x and k_y, and propagate towards left. For $\theta_{inc}>\theta_{ref}$, instead, refracted SWs carries a positive and negative of k_x and k_y value, respectively, and θ_{ref} is larger than 90°. Even if the wavevector of refracted SWs directs toward MD1, the refracted wave propagates into MD2 because the group velocity is still directed toward left, and as a consequence a negative SWs refraction occurs.

Besides single DW, series of periodically distributed magnetic DWs [80] and regular patterns of SDs [81] were also proposed as the basis for MCs to control SWs propagation. Theoretical calculations and micromagnetic simulations showed that in this kind of structures the periodic modulation of the internal field causes a partial reflection of SWs at the DWs inducing the appearance of magnonic band gaps in the SW band diagram. In particular, SDs have been proposed to realize reconfigurable SWs devices exploiting the fact that the orientation of the stripe pattern is not fixed but only depends on sample history [82]. In

fact, the whole stripe pattern develops parallel to the last in-plane saturation direction, and it can be coherently rotated applying a magnetic field perpendicular to the stripe axis [83,84].

C. Banerjee et al. [85] used wave-vector resolved conventional BLS and micromagnetic simulations to study SWs propagation Co/Pd multilayer system developing a SD pattern at remanence (Figure 17 (a)). The micromagnetic simulations of Figure 17 (b) show the spin configuration in details. The authors show that the periodic modulation of the SDs magnetization acts as a periodic potential for SWs propagation, similarly to artificial magnonic crystals, such as arrays of magnetic dots, stripes or antidots prepared by lithografic techniques [86,87].When the SDs pattern is present, the BLS spectra become very rich, and several SWs modes, having different spatial localization in specific regions of the SDs, appear. In addition, the dispersion relation is observed to strongly depends on the angle between the SWs wavector and the stripe axis (Figure 17 (c), (d)), as in one-dimensional magnonic crystals consisting of lithographic patterned magnetic stripes.

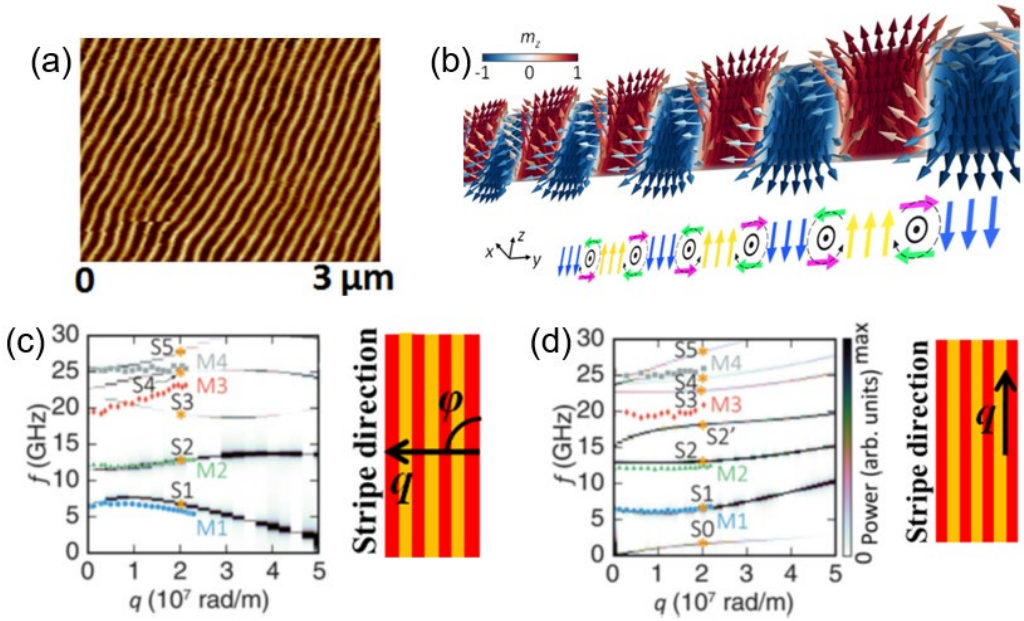

Figure 17. SWs in a stripe domain system. (a) MFM image of stripe domains in a Co/Pd multilayer. (b) Micromagnetic simulation of the spin configuration within the stripes (cross-section). The arrows correspond to the magnetization. (c)-(d) SWs dispersion curves when the wavevector is perpendicular (c) or parallel (d) to the stripes. [85]

More recently, C. Liu et al. [88] investigated SWs propagation in a SDs pattern occurring in $La_{0.67}Sr_{0.3}MnO_3$ (LSMO) films, using propagating spin-wave spectroscopy and micromagnetic simulations.

As it can be seen in Figure 18 (a) the investigated sample consist of 150-nm-thick LSMO film grown on a $LaAlO_3$ substrate and developing a SDs pattern having a periodicity of about 220 nm.

For SWs propagation along the stripes axis, two modes are observed in the experiment. Micromagnetic simulations indicate that low-frequency SWs mode is located both in the domain walls and at the domain surface, while the high-frequency mode is present only in the domain volume, and can be seen as an

effective antiferromagnetic spin-wave mode. In addition, the authors experimentally prove a reprogrammable reorientation of the SDs by the application of an electrical current pulses along the stripes axis (Figure 18 (c), (d)). The SDs pattern doesn't change up to 20 mA, while it coherently rotates along the direction perpendicular to the current direction with an applied current of 25 mA. One can see in Figure 18 (h)-(j) that after current pulses of 10 mA and 20 mA, the amplitude of the SWs transmission signals remain almost constant to the initial value before the current application. However, when current pulse of 25 mA is applied, the spin-wave transmission signal disappears, due to the SDs reorientation. The corresponding magnetization at remanence after the current pulses is shown in Figure 18 (e)-(g). These findings demonstrate the possibility to switch the spin-wave transmission from 'on' to 'off' using a current pulse.

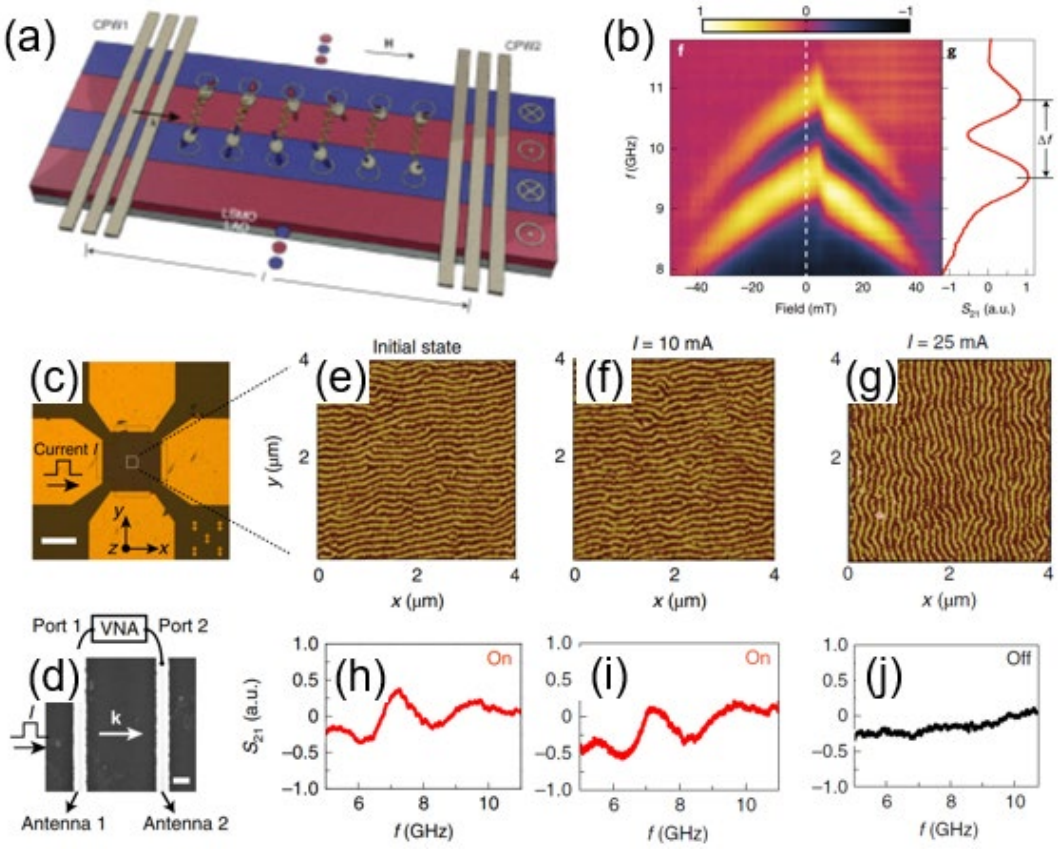

Figure 18. Current-controlled SWs in a stripe domain system. (a) Sketch of the sample system, consisting of an LSMO layer with alternated upward-downward domains. Coplanar waveguides allow for the SW excitation and detection. (b) SWs transmission spectra Im(S_{21}) measured via VNA on the system in (a). (c) Optical image of the device used for the current control of SW. (d) SEM of the device with integrated antennas for SW excitation and detection. (e)-(g) MFM image at remanence of the magnetic configuration in the initial state (e) and after a 10 mA current pulse (f) and 25 mA current pulse (g). (h)-(i) SW transmission signals corresponding to the above panels. In (j) the SW transmission is switched off. [88]

Finally, skyrmion crystal (SkX) phase has been also demonstrated as an effective tool to control the propagation of the spin excitations**.** Magnetic skyrmions are topologically protected spin configuration, which can develop both in chiral magnets and in magnetic multilayers in the presence of the bulk and

interfacial DMI, respectively [89]. In three-dimensional systems, skyrmions can develop string structures extended in the third dimension and composed by the uniform stacking of two-dimensional skyrmions along the string direction. In a very recent study Seki et al. [90] experimentally showed a non-reciprocal propagation of spin excitations along skyrmion strings in the chiral-lattice magnet Cu_2OSeO_3 (Figure 19 (a)) By means of propagating spin-wave spectroscopy measurements the authors investigated the propagation properties of the three magnetic resonance modes supported by the skyrmion crystal phase, namely the clockwise (CW) and the counter-clockwise (CCW) rotational modes and the breathing (B) mode (Figure 19 (b)). A non-reciprocal propagation is observed for all the three investigated modes, and the degree of non-reciprocity, as well as the group velocity and the decay length, were found to be strongly dependent on the excitation character. Such experimental findings were confirmed by the calculated dispersion relations. In addition, a decay length larger than 50 µm was found for low temperature, showing that spin excitations on the skyrmion strings can propagate over a distance 10^3 times the diameter of single skyrmion string which is about 50 nm. This work opens good perspectives for using topologically protected skyrmion strings for unidirectional information transmission lines.

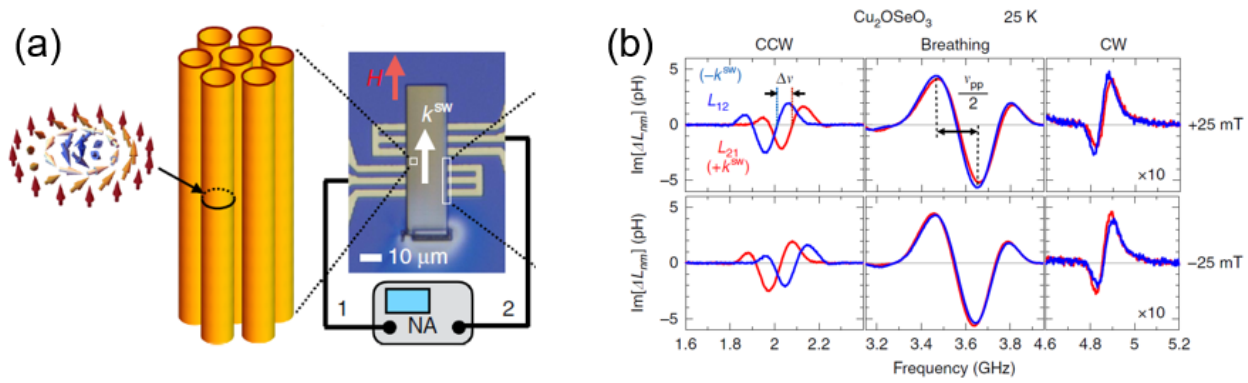

Figure 19. Propagation of spin excitations along skyrmion strings. (a) Left: sketch of the spin configuration of skyrmion strings in Cu_2OSeO_3. Right: optical image of the device, where coplanar waveguides are used to excite and detect the propagating spin dynamics. (b) Spectra of mutual inductance which carry information on the propagating character of the dynamic modes of the strings. [90]

6. Complex systems and devices and future applications

As we mentioned, a wide range of different strategies for the generation, guidance and manipulation of spin waves via spin textures have been demonstrated in the past years. By combining such elements, more complex functionalities and devices can be envisioned. Here we focus on such applications and present both theoretical proposals and experimental works.

6.1 Complex Interaction with Domain walls

In order to increase the energy efficiency of magnonic devices, it is highly desirable to implement functionalities which are fully carried out in the SW domain, i.e. without inefficient interconversion steps. In this framework, in [91], a device is presented allowing for the control of the SW propagation by means of DWs, and the displacement of DWs with magnons. Coherent spin waves with a well-defined wavelength are excited using coplanar waveguides, propagate within a 6 μm wide Ti(8)/Pt(7)/[Co(0.4)/Ni(0.35~0.4)]$_9$/Ru(3) magnetic channel with perpendicular magnetic anisotropy, and are detected inductively using a second coplanar waveguide and a vector network analyzer. By properly initializing the magnetic configuration with external fields, a single DW was nucleated in between the two coplanar waveguides. The authors show experimentally that the spin waves transmitted across the domain wall exhibit a roughly 180° phase shift (Figure 20 (c)), with respect to the case where no domain wall is present (Figure 20 (b)). The results of micromagnetic simulations confirm this effect, showing the spin wave phase as a function of distance from the antenna, for the case where the DW is present (Figure 20 (a), bottom panel), and absent (Figure 20 (a), top panel).

Conversely, it is also shown that large amplitude SWs impinging on the domain wall displace it towards the SWs source, consistently with a magnonic spin-transfer torque induced switching mechanism. Figure 20 (d) shows the Kerr images before and after the SW pulse, which show the SW-induced DW displacement. The SW-induced DW displacement mechanism is further studied quantitatively in Figure 20 (e), where the corresponding change in the domain switching field associated to the presence (bottom panel) or absence (top panel) of the spin waves, is shown. This provides an intriguing demonstration of the possibility of using spin textures for modulating spin waves, and spin waves for reconfiguring the domain structure, in a single device.

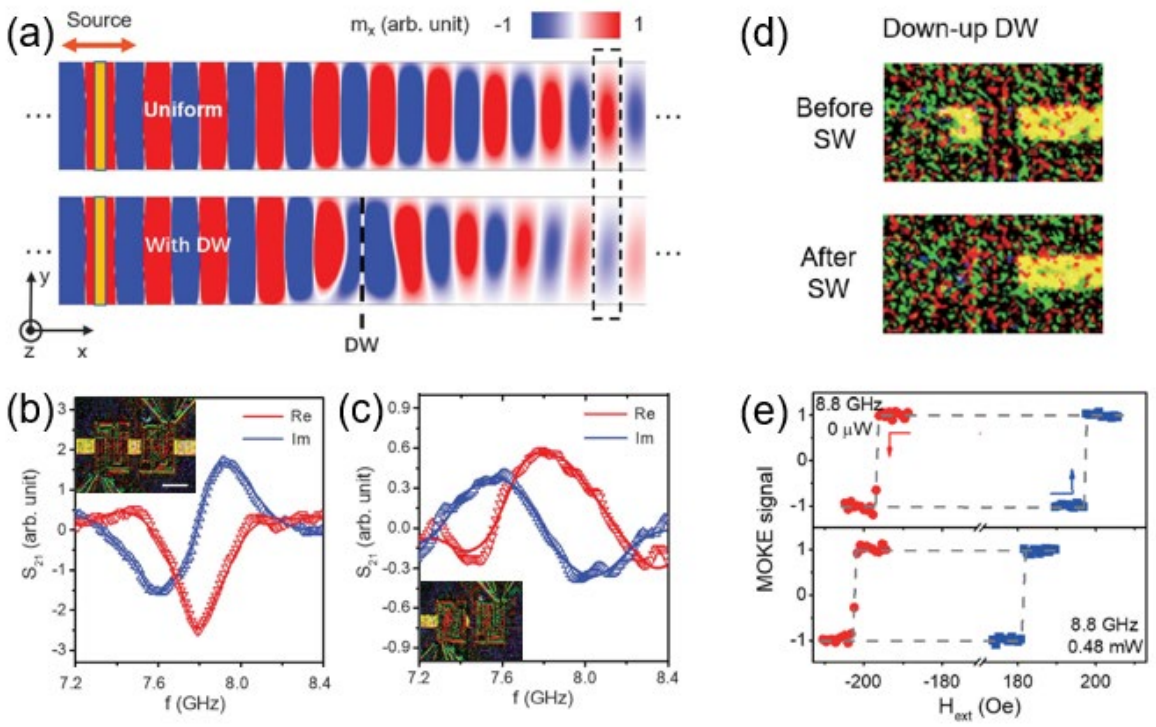

Figure 20. Mutual control of domain walls and SWs. (a) Simulated propagation of SWs in a Co/Ni multilayer 600 nm wide slab with perpendicular magnetic anisotropy, in absence (top panel) and presence (bottom panel) of the domain wall. SWs are excited and detected using coplanar waveguides. (b)-(c) Mutual inductance S_{21} spectra in the case of absence (b) and presence (c) of the domain wall between the antennas, showing a nearly 180° phase shift of spin waves passing through the wall. (d) Kerr microscopy images showing the SW-induced domain wall displacement. (e) SW-induced change in the switching field at the location of the DW. [91]

The nonlinear interaction of propagating SWs with a single DW is studied in [92], where the authors show analytically and via simulations that a SW frequency comb can be realized. The authors show that travelling SWs strongly interact nonlinearly with an oscillating DW giving rise to the emission of a comb-like spectrum. The theoretical explanation lies in the framework of nonlinear magnon scattering between the traveling magnons and the high-density magnons generated by the DW oscillation. The system investigated is a 10 nm thick, 50 nm wide magnetic nanostrip where a tail-to-tail Néel wall is stabilized via shape anisotropy. The wall is set in oscillation at the f_{DW} frequency via a localized RF external field applied in the region of the wall, while propagating SWs are emitted via an "input" line RF field at f_{SW} excitation at the beginning of the stripe. The output region where the SW spectrum is analyzed is located on the opposite end of the nanostrip with respect to the wall. The authors observe an output SW frequency comb spectrum with a main peak at f_{SW} and sharp side peaks corresponding to $f_{SW}+N*f_{DW}$ and $f_{SW}-N*f_{DW}$. The relative intensity of the peaks can be controlled with the domain wall oscillation.

Recently, Qin et al. [93] reported the experimental demonstration of an active manipulation of propagating SWs by means of electric-field controlled ferroelectric domain wall motion in a strain-coupled Fe/$BaTiO_3$ heterostructure. The investigated sample is a Fe film, 26 nm thick, grown on a ferroelectric $BaTiO_3$(001) substrate consisting of alternating domains with in-plane and perpendicular polarization, indicated as *a* and *c* domains, respectively (see Figure 21 (a)). As it can be seen in the MOKE microscopy measurements, a modulation of the magnetic anisotropy is induced in the Fe film by strain transfer from the ferroelectric domain pattern. In particular, Fe regions located on top of the *a* (*c*) domains are characterized by a uniaxial (biaxial) in-plane anisotropy with the easy direction parallel (oriented at 45°) with respect to the ferroelectric domain walls. The authors investigated the SWs propagation in a *c*–*a*–*c* domain structure by means of super-Nyquist sampling magneto-optical Kerr effect (SNS-MOKE) microscopy measurements. A microwave antenna was used to excite SW in the first *c* domain, while an external magnetic field of 70 mT was applied along the ferroelectric domain walls in order to saturate the magnetization along the direction perpendicular to the SW wavevector (corresponding to the DE geometry) in both the *a* and *c* domains.

In zero electric field, the two *c* domains are separated by an *a* domain having a width of 14 μm. For an excitation frequency lower than the FMR frequency in the *a* domain (*f*=10.5GHz), the absence of propagating modes in the *a* domain causes strong SW reflection at the *c*–*a* boundary, and the SW amplitude is suppressed in the *a* domain over a distance of 14 μm. When the excitation frequency is increased to 12.0 GHz, instead, a FMR-like mode ($k \approx 0$) in the *a* domain, promotes the transmission of SWs into the second *c* domain. For higher frequencies, instead, SWs can efficiently propagate in both the *a* and *c* domains. In addition a conversion of the SW wavelength was observed at the *c*–a and *a*–*c* anisotropy boundaries, due to the different SW dispersion relation in the *a* and *c* domains. When an electric field of 1 kV/cm is applied perpendicular to the surface sample across the $BaTiO_3$ substrate, the *c* domains grow at the expense of the *a* domains via lateral motion of the ferroelectric domain walls and the width of the central *a* domain reduces to about 5.5 μm. Since the magnetic anisotropy boundaries in the Fe film are pinned onto the ferroelectric domain walls in $BaTiO_3$, they are forced to move accordingly. Very interestingly, the application of the electric field across the $BaTiO_3$ substrate was found to tune both the amplitude and phase of propagating spin waves in the Fe film. Figure 21 (b)-(g) show the SNS-MOKE images of spin waves at different frequencies and applied voltages. For *f*=10.5 GHz the suppression of the SW amplitude is observed for over a length of only 5.5 μm due to the reduction of the width of the *a* domain. For $f \geq 12$ GHz SWs are observed to propagate across the c–a–c domain structure, acquiring a negative phase shift compared to SWs propagating over the same distance in a single c domain. This can be observed in Figure 21 (h) reporting the absolute value of phase change $\Delta\phi = |\phi - \phi_{ref}|$ as a function of the width of the *a* domain (w_a), where ϕ is the phase detected beyond the *a* domain at y=25 μm and ϕ_{ref} is the reference phase at the same position for a single *c* domain. Both experimental data and simulations show a linear increase of $\Delta\phi$ on increasing the width of the *a* domain. In particular, it is observed that the electric field only needs to change the size of the a domain by 1.3 μm to induce a phase shift of π. Moreover, the authors find that when the voltage is turned off, the magnetic anisotropy boundaries slowly move back to their initial position because of strain relaxation in $BaTiO_3$, demonstrating a reversible modulation of the SW phase and amplitude. These findings demonstrate a new control

mechanism, which provides independent tuning of the amplitude and phase of propagating SWs, opening new prospects toward the implementation of SW-based logic devices.

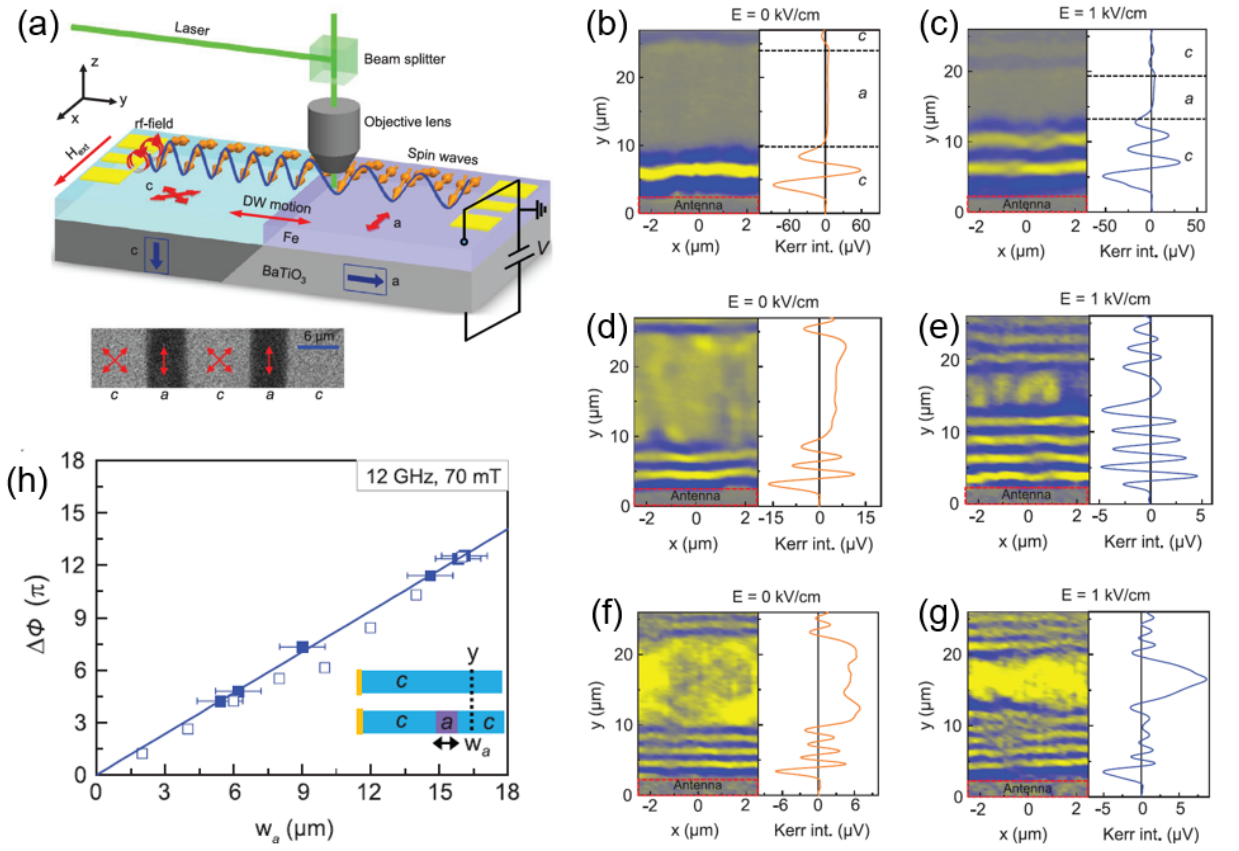

Figure 21. Electric-field control of SWs via ferroelectric domain wall motion. (a) Sketch of the investigated sample, consisting of a 26 nm Fe / BTO stack with alternated in-plane and out-of-plane polarization domains. SWs are emitted and detected using RF antennas, and visualized via Kerr microscopy. (b)-(g) Kerr images of propagating SWs and corresponding line profiles for E=0 kV/cm (left panels) and E=1kV/cm (right panels). The SW frequency is 10.5 GHz (b), (c), 12.0 GHz (d), (e), and 13.5 GHz (f), (g). (h) SW phase-change as a function of the width of the a-domain width, at 12.0 GHz and 70 mT. Open and solid symbols are simulations and experiments. [93]

6.2 Combined Emission and Guidance

Another appealing feature is the combination of two of the basic building blocks introduced before, i.e. SW generation and guidance, using spin textures. In [94,95] it is demonstrated the injection and propagation of SWs emitted by a vortex core into a DW based waveguide, and into a 2D network composed of DWs, respectively.

In the first work [94], a hybrid structure (Figure 22 (a)) comprising a 50 nm thick Py rectangular strip grown on top of a 50 nm thick Py nanodisk is employed. Due to the shape anisotropy, a Néel domain wall and a vortex are stabilized in the strip and nanodisk, respectively. SWs in the 6-12 GHz range are emitted by exciting the radial vortex modes with an out-of-plane oscillating external field, and propagate within the domain wall. By using micro-focused BLS, the authors measure the 2D map of the SW intensity and extract the exponential decay profile as SWs propagate along the domain wall away from the source, and demonstrate SW confinement in the transverse direction at the domain wall (Figure 22 (b)).

In the second work [95], the authors stabilize a 2D vortex network in a 30 nm thick nanopatterned Py stripe, and fabricate an "omega" shaped stripline for exciting the oscillation of a single vortex core via out-of-plane fields in the 1-4 GHz range. Figure 22 (c) shows a sketch of the sample structure. Then, they observe with high spatial and temporal resolution the out-of-plane component of the magnetization associated with the propagating SWs via time-resolved STXM. The snapshot reported in Figure 22 (d) shows that radial wavefronts are emitted by the oscillating core, couple with the domain wall bound modes and propagate within the 2D domain wall network. Remarkably, SWs with a short wavelength of around 125 nm at 4 GHz propagate within the network displaying a decay length of several microns.

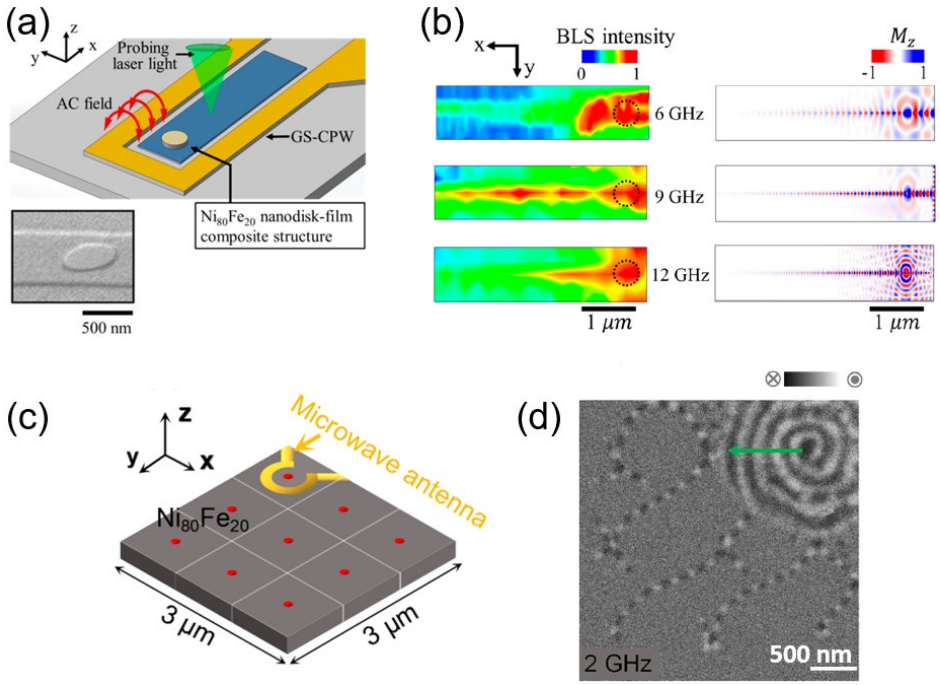

Figure 22. Combined SW emission and guidance via spin textures. (a)-(b) SWs are emitted by a vortex core and injected in a domain wall. A nanodisk-film composite structure (a) is used for stabilizing the vortex and wall. An RF antenna is used for SW excitation and BL microscopy for SW detection. μ-BLS measurements and simulations (b) show the tunable SW emission by the core and channeling within the wall at 6 GHz, 9 GHz and 12 GHz. [94] (c)-(d) SWs are emitted by a vortex core and guided in a 2D network of DWs. The sketch of the sample (c) shows the vortex network, with an omega shaped antenna for exciting the core dynamics. SWs at 2 GHz channeled in the domain walls and propagating are studied via time-resolved STXM (d) [95].

6.3 Devices based on antiferromagnetic spin textures

Despite the study of antiferromagnetic materials for magnonics is still at its infancy, antiferromagnets are raising considerable attention due to their several potential advantages with respect to ferromagnets. In fact, they support magnons with different polarization, they typically have higher resonant frequencies (THz), are resilient to external magnetic fields, and don't have stray fields. In this framework, it is possible to design complex device functionalities which are specifically enabled by the use of spin textures in antiferromagnetic materials.

In [96], the authors show theoretically and with micromagnetic simulations that an antiferromagnetic domain wall in presence of DMI can be used both as a spin-wave polarizer, i.e. a device able to create a specific linear polarization, and a retarder, i.e. a device able to convert between linear and circular polarization. The physical mechanism beyond both these effects is the fact that the spin-wave scattering at the antiferromagnetic domain wall, in presence of DMI, is dependent on the polarization of the impinging SW. At lower SW frequencies, this translates in a different transmission coefficient of in-plane and out-of-plane SW modes, leading to the typical "polarizer" behavior similarly to photons. At higher frequency however, the transmission coefficient is close to 1 for both modes, but due to the different effective potential experienced at the wall, a phase delay is developed between the two modes, leading to the "retarder" behavior. Figure 23 (a) shows a schematic representation of the "polarizer" functionality.

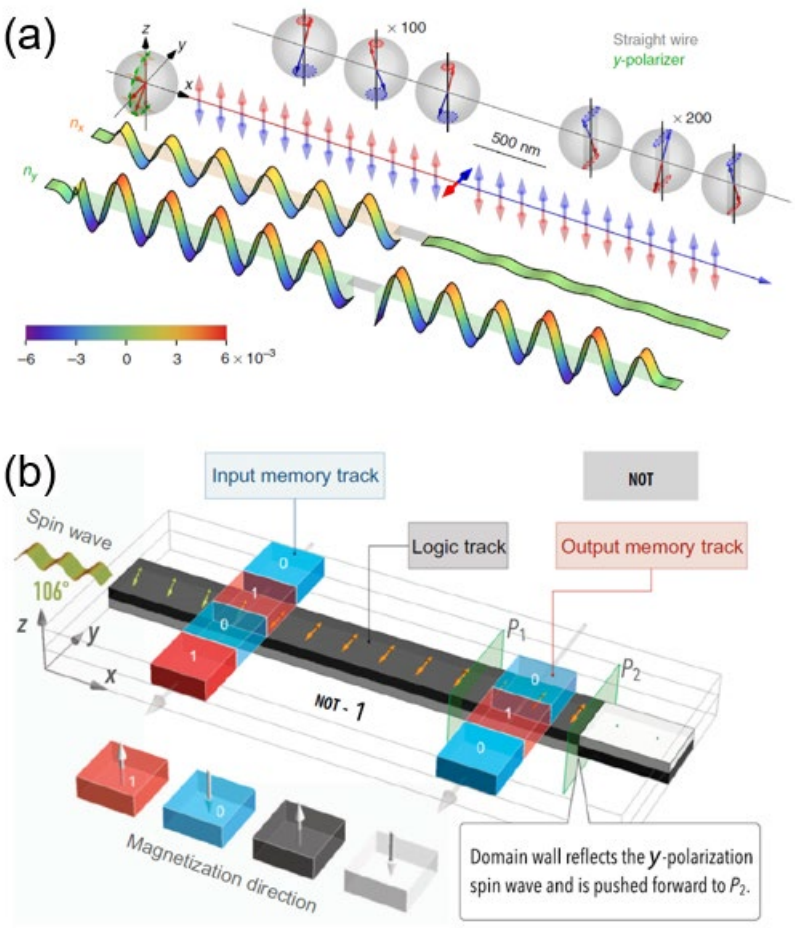

Figure 23. Magnonic devices based on antiferromagnetic spin textures. (a) Sketch of a SW polarizer consisting of an antiferromagnetic domain wall in a straight wire. Top row: SWs on Bloch spheres. Second row: static magnetization profile. Third-bottom row: only the SWs with y-polarization impinging on the domain wall are transmitted. [96] (b) Proposal for a NOT gate using SWs traveling in a synthetic antiferromagnet wire with a domain wall [97]

By exploiting once again the interplay between polarized spin waves and domain walls in antiferromagnets, the same authors propose a design for a universal logic gate [97], analogue to a Datta-Das spin transistor [98] for SWs. In particular, the authors combine two effects, namely a magnetic gating effect, for controlling the SW polarization via static magnetic domains, and the polarization-dependent domain wall motion [99], for controlling the domain structure via SWs. As a result, they propose the design for a set of fully magnetic logic gates with integrated memory, where the information is stored in static domains, converted into the SW polarization state via gating, processed and finally converted back to the static domain state. Figure 23 (b) shows the schematic of a proposed NOT logic gate based on antiferromagnetic SWs propagating within a synthetic antiferromagnetic wire. It consists of two racetrack memories connected via a synthetic antiferromagnetic wire. The input bits are stored as UP or DOWN magnetic domains in the racetrack, which act as a magnetic gate for the polarization of antiferromagnetic SWs propagating in the synthetic antiferromagnet underneath. The bit is therefore encoded in the SW

polarization, and transported towards the output. The output exploits the fact that, due to the polarization-dependent DW motion effect, a DW is “pushed” only when the SW was gated with bit 1, and stays still when the SW was gated with bit 0. The resulting magnetization is finally used for imprinting the magnetic state in the output racetrack. By generalizing this concept the authors propose a design for a universal logic gate.

6.4 Spin-wave circuits and devices

Starting from the rich phenomenology associated with the SW confinement at DWs, several studies have proposed the realization of complex DW-based circuits and networks for allowing the steering and interference of SWs.

Particularly appealing for applications is the case of chiral DWs stabilized in perpendicularly magnetized ferromagnets in presence of interfacial DMI. In [100], the authors theoretically propose a design that makes use of Nèel-type domain walls stabilized in 300 nm x 60 nm slab made of perpendicularly magnetized material with interfacial DMI, as building blocks for a magnonic logic architecture. The presence of the DMI is crucial for both setting the chirality of the wall, and allowing the wall stabilization in narrow slabs. In particular, they encode the logic states in the presence (0 state) or absence (1 state) of the wall within the slab. The spin texture can be controlled by using local external fields or spin polarized currents for switching the spin state of the slab from a multidomain state which contains the DW, to a monodomain state. SWs are excited and detected by using a couple of antennas located at the two extremities of the slab. The working principle of the logic gates exploits the fact that DW-bound SWs can be excited in a frequency range which lays within the bulk bandgap, and therefore the SW transmission is strong in the 0 state and absent in the 1 state. The designs for the NAND gate uses two slabs in parallel, which represent the individual inputs, and the total integrated SW signal as output. Only when both slabs are in the DW state, the output SW signal would be strong, corresponding to the logic ‘1’ output.

The versatility and robustness of chiral Nèel walls allows envisioning the realization of reconfigurable channels where SWs are guided and let interfere. In [101] the authors present theoretically a strategy for building 2D spin-wave networks by combining chiral Nèel walls and chiral excitation of exchange SWs in out-of-plane magnetized TmIG thin films. In particular, by placing 2 parallel ferromagnetic nanowires perpendicular to the DW, and providing RF excitation, unidirectional emission of wall-bound SWs is induced [102]. Applying this concept, the authors present a prototypical 800 nm diameter ring-shaped structure hosting a single “circle-shaped” DW, demonstrating via micromagnetic simulations the efficient unidirectional emission and guidance of SWs from the input region to the output region located on the other side of the ring. By combining multiple rings to form an antidot lattice, and integrating multiple input nanowires, the authors build a reconfigurable 2D SW network which is also used for demonstrating basic SW-based logic functionality. In fact, in a 2 x 2 antidot lattice with 4 input/output terminals (one per dot), the authors show the possibility to reconfigure the connections of the terminals by changing the location of the domain walls.

The same 2x2 antidot lattice is used for demonstrating XNOR logic functionality (Figure 24 (a)). SWs are emitted in the 2 input regions, so that the logic states are encoded in the SW phase, and travel within the same DW until the output region, where the SW amplitude is measured. By traveling in the same nanochannel, SWs interfere constructively or destructively depending on their initial phase difference, so that the output amplitude is maximum (logic 1) only when the initial phases are both 0 or π (Figure 24 (b), (c)). A majority gate is demonstrated using similar concepts in a 3x3 antidot lattice.

With a similar strategy, in [103], the authors present a design for realizing 2D spin wave circuits using Bloch DWs in presence of DMI, in in-plane magnetized films. The peculiarity of such system is that SWs confined and propagating within the DWs are spatially shifted on the right or on the left with respect to the DW center, depending on their propagation direction. This shift is used as the basic principle of a "spin-wave diode". In this design, the spin waves propagating within the circuit in the "forward direction" (Figure 24 (d), (e)) are guided efficiently and reach the output terminal, whereas the spin waves propagating in the "reverse direction" (Figure 24 (f), (g)) are spatially shifted away and do not couple efficiently with the output terminal. Given that the direction and entity of the spatial shift is related to the sign and magnitude of the DMI, the authors propose to introduce reconfigurability by tuning in real-time the DMI by static electric fields [104]. This would lead to controlling in real time the diode characteristics. Furthermore, the circuit geometry itself could be shaped by displacing the domain wall positions via external fields, currents or magnons.

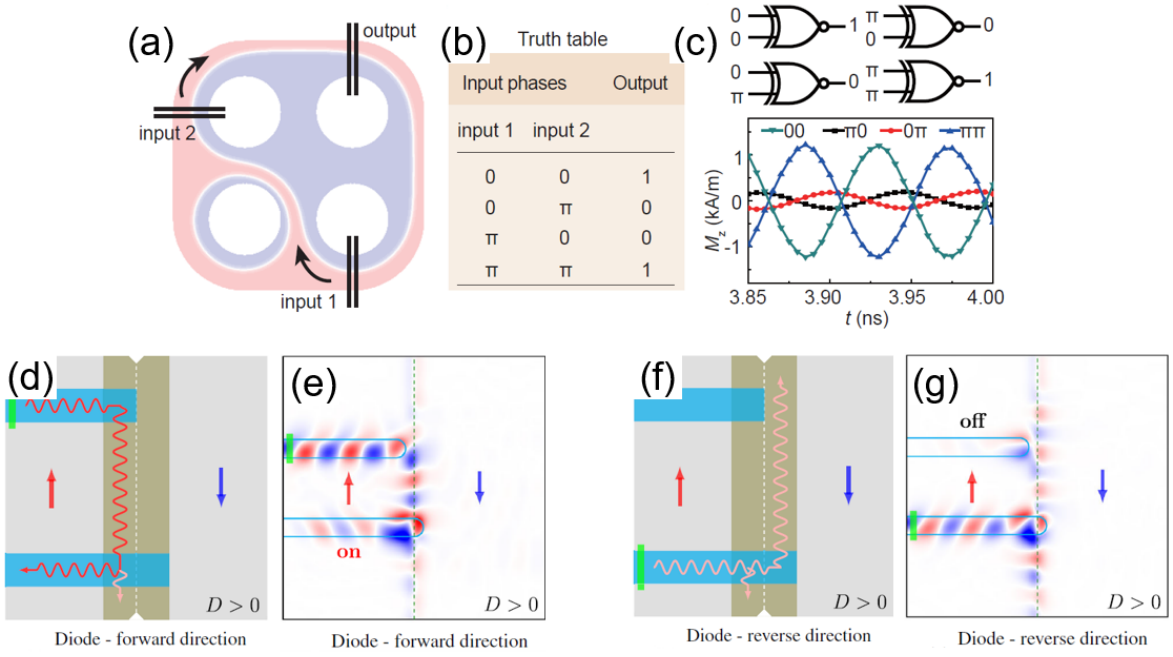

Figure 24. Complex SW circuits based on spin textures. (a)-(c) Sketch of a proposal for a XNOR Logic Gate based on chiral domain wall waveguides (a), using the SW phase as logic input and the resulting SW amplitude after interference as logic output. The truth table (b) and the time-dependent magnetization component (c) are shown [101]. (d)-(g) Design and simulations of a SW diode using domain wall waveguides, in presence of DMI. In the forward direction (d)-(e) SWs are transmitted from the lower to the upper terminal. In the reverse direction (f)-(g) the SWs are blocked due to the DMI-induced spatial displacement of the SWs [103].

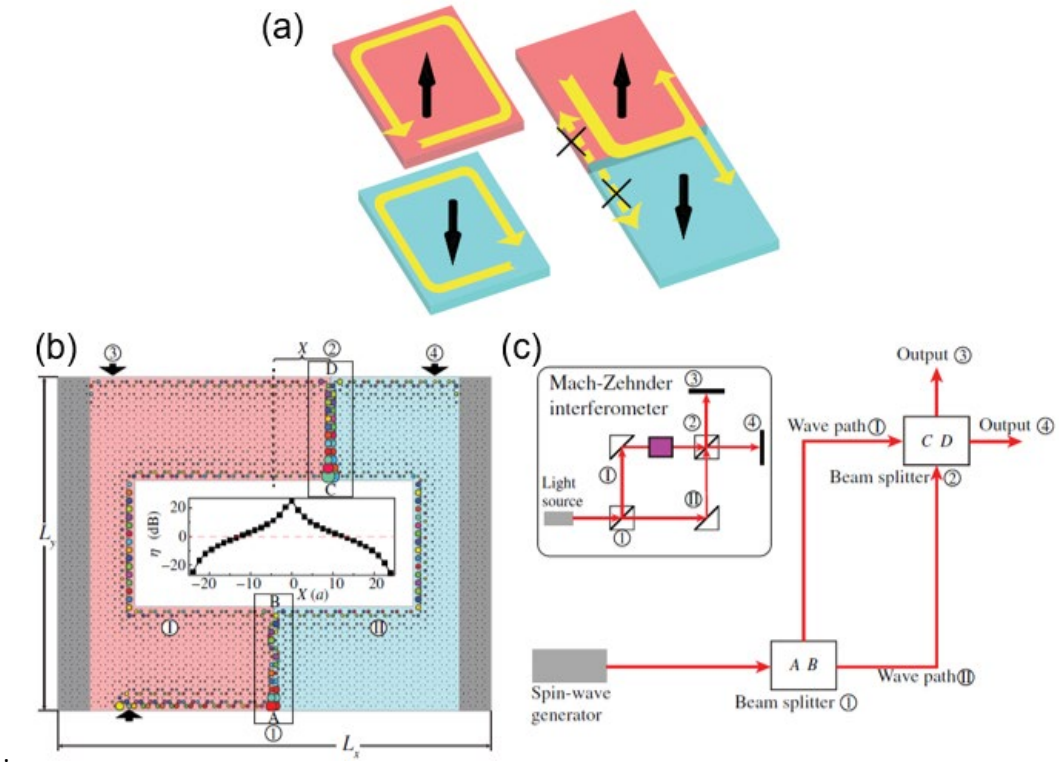

Figure 25. Magnonic circuits and devices based on topologically protected exchange SWs. (a) Schematic image of the topological exchange SW modes localized at the sample edges (left) and at the domain walls (right). Red and blue regions indicate upward and downward magnetization direction. Yellow arrows mark the propagation direction of the SWs. (b) Proposal for a SW Mach-Zehnder interferometer, where a SW beam is generated in 1, travel along a domain wall, are split in two paths, recombined in 2 and finally the outputs in 3 and 4 depend on the SW interference. (c) Schematic of the corresponding optical interferometer. [105]

In [105], the concept of "topological magnonics" is presented. Here, a plethora of possible device implementation are proposed that make use of the specific advantages associated with topologically protected spin wave modes [106,107]. The authors propose to use a ferromagnetic layer with perpendicular magnetic anisotropy on a honeycomb lattice which, in presence of DMI, exhibits topological magnonic properties. In such system, there exist topologically protected chiral spin-wave modes which lay in the bandgap of bulk modes, and lead to the unidirectional spin-wave propagation along the sample edges or at the magnetic domain walls (Figure 25 (a)). The propagation direction of such modes is locked to the direction of the magnetization of the bulk, which means that the magnetization orientation and domain structure can be used as a convenient knob for controlling the functionality and geometry of the circuit. The authors use such properties for designing a spin-wave diode, a beam splitter and a Mach-Zehnder interferometer (Figure 25 (b), (c)), simply by controlling the magnetic domain structure. For example, a single sample edge or domain wall represents a diode, due to the unidirectionality of SW propagation. Interestingly, the fact that the functionality is determined by the magnetic domain structure allows to reconfigure the device on demand.

Conclusions

The extremely rich phenomenology involving the interaction of SWs and spin textures ranges from the SW confinement and guidance, to the emission of shaped wavefronts, to the spatial manipulation of the phase, amplitude, reflection, refraction and interference, to nonlinear effects. From these "building blocks", complex devices can be envisioned which exploit these unique characteristics, for implementing Boolean or non-Boolean computing concepts.

Among these last, a promising avenue lays in the study of non-conventional computing architectures, such as machine-learning based methods [108–110], which could strongly benefit by the additional degree of freedom given by the control of the spin texture.

Another interesting aspect for future study, is the use of spin textures as a gateway to realize fully-magnonic devices, by either exploiting non-linear effects triggered by nanoscale spin textures, or by exploiting the interaction of magnons for reconfiguring the magnetic domain structure. The possibility to avoid lossy interconversions from the magnon domain to the electronics is indeed needed to realize energy efficient devices.

On the materials side, so far the investigation has involved mainly ferromagnetic materials. However, SWs in antiferromagnetic materials however possess important advantages, among which higher working frequencies and tunable polarization. Exploring experimentally the interaction of SWs with spin textures in such systems represents largely unexplored territory, due to the inherent experimental difficulties in exciting and detecting SWs in antiferromagnets.

Engineered spin textures represent a novel avenue for designing and realizing complex functionalities in magnonic devices. Despite being still at its infancy, a plethora of theoretical and experimental results across a wide range of materials, techniques and applications testify the strong activity and promise of this exciting field.

Acknowledgements

This research was funded by the European Union's Horizon 2020 research and innovation programme under grant agreement number 948225, project B3YOND. This work was partially performed at PoliFAB, the micro- and nano-technology center of the Politecnico di Milano.

References

[1] Parkin S S P, Hayashi M and Thomas L 2008 Magnetic domain-wall racetrack memory *Science (80-.).* **320** 190–4

[2] Fert A, Cros V and Sampaio J 2013 Skyrmions on the track *Nat. Nanotechnol.* **8** 152–6

[3] Pribiag V S, Krivorotov I N, Fuchs G D, Braganca P M, Ozatay O, Sankey J C, Ralph D C and Buhrman R A 2007 Magnetic vortex oscillator driven by d.c. spin-polarized current *Nat. Phys.* **3** 498–503

[4] Mistral Q, Van Kampen M, Hrkac G, Kim J Von, Devolder T, Crozat P, Chappert C, Lagae L and Schrefl T 2008 Current-driven vortex oscillations in metallic nanocontacts *Phys. Rev. Lett.* **100** 1–4

[5] Chumak A V., Vasyuchka V I, Serga A A and Hillebrands B 2015 Magnon spintronics *Nat. Phys.* **11** 453–61

[6] Pirro P, Vasyuchka V I, Serga A A and Hillebrands B 2021 Advances in coherent magnonics *Nat. Rev. Mater.* **6** 1114–35

[7] Barman A, Gubbiotti G, Ladak S, Adeyeye A O, Krawczyk M, Grafe J, Adelmann C, Cotofana S, Naeemi A, Vasyuchka V I, Hillebrands B, Nikitov S A, Yu H, Grundler D, Sadovnikov A V., Grachev A A, Sheshukova S E, Duquesne J Y, Marangolo M, Csaba G, Porod W, Demidov V E, Urazhdin S, Demokritov S O, Albisetti E, Petti D, Bertacco R, Schultheiss H, Kruglyak V V., Poimanov V D, Sahoo S, Sinha J, Yang H, Münzenberg M, Moriyama T, Mizukami S, Landeros P, Gallardo R A, Carlotti G, Kim J V., Stamps R L, Camley R E, Rana B, Otani Y, Yu W, Yu T, Bauer G E W, Back C, Uhrig G S, Dobrovolskiy O V., Budinska B, Qin H, Van Dijken S, Chumak A V., Khitun A, Nikonov D E, Young I A, Zingsem B W and Winklhofer M 2021 The 2021 Magnonics Roadmap *J. Phys. Condens. Matter* **33** 413001

[8] Yu H, Xiao J and Schultheiss H 2021 Magnetic texture based magnonics *Phys. Rep.* **905** 1–59

[9] Ross C 2001 Patterned Magnetic Recording Media *Annu. Rev. Mater. Res.* **31** 203–35

[10] Kleiber M, Kümmerlen F, Löhndorf M, Wadas A and Weiss D 1998 Magnetization switching of submicrometer Co dots induced by a magnetic force microscope tip *Phys. Rev. B* **58** 5563

[11] Kent N, Reynolds N, Raftrey D, Campbell I T G, Virasawmy S, Dhuey S, Chopdekar R V., Hierro-Rodriguez A, Sorrentino A, Pereiro E, Ferrer S, Hellman F, Sutcliffe P and Fischer P 2021 Creation and observation of Hopfions in magnetic multilayer systems *Nat. Commun. 2021 121* **12** 1–7

[12] Shinjo T, Okuno T, Hassdorf R, Shigeto K and Ono T 2000 Magnetic vortex core observation in circular dots of permalloy *Science (80-.).* **289** 930–2

[13] Gilbert D A, Maranville B B, Balk A L, Kirby B J, Fischer P, Pierce D T, Unguris J, Borchers J A and Liu K 2015 Realization of ground-state artificial skyrmion lattices at room temperature *Nat. Commun.* **6** 1–7

[14] Li J, Tan A, Moon K W, Doran A, Marcus M A, Young A T, Arenholz E, Ma S, Yang R F, Hwang C and Qiu Z Q 2014 Tailoring the topology of an artificial magnetic skyrmion *Nat. Commun. 2014 51* **5** 1–6

[15] Grujicic D and Pesic B 2005 Micromagnetic studies of cobalt microbars fabricated by nanoimprint lithography and electrodeposition *J. Magn. Magn. Mater.* **285** 303–13

[16] Mcgrouther D, McVitie S, Chapman J N and Gentils A 2007 Controlled domain wall injection into ferromagnetic nanowires from an optimized pad geometry *Appl. Phys. Lett.* **91** 022506

[17] Fassbender J, Ravelosona D and Samson Y 2004 Tailoring magnetism by light-ion irradiation *J. Phys. D. Appl. Phys.* **37**

[18] Chappert C 1998 Planar Patterned Magnetic Media Obtained by Ion Irradiation *Science (80-.).* **280** 1919–22

[19] Kim S, Lee S, Ko J, Son J, Kim M, Kang S and Hong J 2012 Nanoscale patterning of complex magnetic nanostructures by reduction with low-energy protons. *Nat. Nanotechnol.* **7** 567–71

[20] McGrouther D and Chapman J N 2005 Nanopatterning of a thin ferromagnetic CoFe film by focused-ion-beam irradiation *Appl. Phys. Lett.* **87** 022507

[21] Makarov D, Tibus S, Rettner C T, Thomson T, Terris B D, Schrefl T and Albrecht M 2008 Magnetic strip patterns induced by focused ion beam irradiation *J. Appl. Phys.* **103** 063915

[22] Albertini F, Nasi L, Casoli F, Fabbrici S, Luches P, Gazzadi G C, Di Bona A, Vavassori P, Valeri S and Contri S F 2008 Local modifications of magnetism and structure in FePt (001) epitaxial thin films by focused ion beam: Two-dimensional perpendicular patterns *J. Appl. Phys.* **104** 053907

[23] Kuepper K, Wintz S, Raabe J, Buess M, Akhmadaliev C, Bischoff L, Quitmann C and Fassbender J 2009 Magnetization dynamics of Landau structures: tuning the response of mesoscopic magneticobjects using defects *J. Phys. Condens. Matter* **21** 436003

[24] Mougin a., Poppe S, Fassbender J, Hillebrands B, Faini G, Ebels U, Jung M, Engel D, Ehresmann a. and Schmoranzer H 2001 Magnetic micropatterning of FeNi/FeMn exchange bias bilayers by ion irradiation *J. Appl. Phys.* **89** 6606–8

[25] Holzinger D, Zingsem N, Koch I, Gaul A, Fohler M, Schmidt C and Ehresmann A 2013 Tailored domain wall charges by individually set in-plane magnetic domains for magnetic field landscape design *J. Appl. Phys.* **114** 013908

[26] Genoni P, Genuzio F, Menteş T O, Santos B, Sala A, Lenardi C and Locatelli A 2018 Magnetic Patterning by Electron Beam-Assisted Carbon Lithography *ACS Appl. Mater. Interfaces* **10** 27178–87

[27] Guang Y, Peng Y, Yan Z, Liu Y, Zhang J, Zeng X, Zhang S, Zhang S, Burn D M, Jaouen N, Wei J, Xu H, Feng J, Fang C, van der Laan G, Hesjedal T, Cui B, Zhang X, Yu G and Han X 2020 Electron Beam Lithography of Magnetic Skyrmions *Adv. Mater.* **2003003** 1–8

[28] De Teresa J M, Fernández-Pacheco A, Córdoba R, Serrano-Ramón L, Sangiao S and Ibarra M R 2016 Review of magnetic nanostructures grown by focused electron beam induced deposition (FEBID) *J. Phys. D. Appl. Phys.* **49** 243003

[29] Jaafar M, Serrano-Ramón L, Iglesias-Freire O, Fernández-Pacheco A, Ibarra M R, de Teresa J M and Asenjo A 2011 Hysteresis loops of individual Co nanostripes measured by magnetic force microscopy *Nanoscale Res. Lett.* **6** 1–6

[30] Garcia R, Knoll A W and Riedo E 2014 Advanced scanning probe lithography. *Nat. Nanotechnol.* **9** 577–87

[31] Howell S T, Grushina A, Holzner F and Brugger J 2020 Thermal scanning probe lithography—a review *Microsystems Nanoeng.* **6** 21

[32] Vettiger P, Brugger J, Despont M, Drechsler U, Dürig U, Häberle W, Lutwyche M, Rothuizen H, Stutz R, Widmer R and Binnig G 1999 Ultrahigh density, high-data-rate NEMS-based AFM data storage system

Microelectron. Eng. **46** 11–7

[33] Albisetti E, Petti D, Pancaldi M, Madami M, Tacchi S, Curtis J, King W P, Papp A, Csaba G, Porod W, Vavassori P, Riedo E and Bertacco R 2016 Nanopatterning reconfigurable magnetic landscapes via thermally assisted scanning probe lithography *Nat. Nanotechnol.* **11** 545–51

[34] Albisetti E, Calò A, Spieser M, Knoll A W, Riedo E and Petti D 2018 Stabilization and control of topological magnetic solitons via magnetic nanopatterning of exchange bias systems *Appl. Phys. Lett.* **113** 162401

[35] Albisetti E, Tacchi S, Silvani R, Scaramuzzi G, Finizio S, Wintz S, Rinaldi C, Cantoni M, Raabe J, Carlotti G, Bertacco R, Riedo E and Petti D 2020 Optically Inspired Nanomagnonics with Nonreciprocal Spin Waves in Synthetic Antiferromagnets *Adv. Mater.* **32** 1906439

[36] Wang Y-L, Xiao Z-L, Snezhko A, Xu J, Ocola L E, Divan R, Pearson J E, Crabtree G W and Kwok W-K 2016 Rewritable artificial magnetic charge ice *Science (80-.).* **352** 962–6

[37] Gartside J C, Arroo D M, Burn D M, Bemmer V L, Moskalenko A, Cohen L F and Branford W R 2018 Realization of ground state in artificial kagome spin ice via topological defect-driven magnetic writing *Nat. Nanotechnol.* **13** 53–8

[38] Takemura Y, Hayashi S, Okazaki F, Yamada T and Shirakashi J I 2005 Direct modification of magnetic domains in Co nanostructures by atomic force microscope lithography *Japanese J. Appl. Physics, Part 2 Lett.* **44** L285

[39] Tejo F, Toneto D, Oyarzún S, Hermosilla J, Danna C S, Palma J L, Da Silva R B, Dorneles L S and Denardin J C 2020 Stabilization of Magnetic Skyrmions on Arrays of Self-Assembled Hexagonal Nanodomes for Magnetic Recording Applications *ACS Appl. Mater. Interfaces* **12** 53454–61

[40] Haykal A, Fischer J, Akhtar W, Chauleau J Y, Sando D, Finco A, Godel F, Birkhölzer Y A, Carrétéro C, Jaouen N, Bibes M, Viret M, Fusil S, Jacques V and Garcia V 2020 Antiferromagnetic textures in BiFeO3 controlled by strain and electric field *Nat. Commun.* **11** 1–7

[41] Lahtinen T H E, Tuomi J O and Van Dijken S 2011 Pattern Transfer and Electric-Field-Induced Magnetic Domain Formation in Multiferroic Heterostructures *Adv. Mater.* **23** 3187–91

[42] Vogt K, Schultheiss H, Jain S, Pearson J E, Hoffmann A, Bader S D and Hillebrands B 2012 Spin waves turning a corner *Appl. Phys. Lett.* **101** 042410

[43] Vogt K, Fradin F Y, Pearson J E, Sebastian T, Bader S D, Hillebrands B, Hoffmann A and Schultheiss H 2014 Realization of a spin-wave multiplexer *Nat. Commun.* **5** 3727

[44] Haldar A, Kumar D and Adeyeye A O 2016 A reconfigurable waveguide for energy-efficient transmission and local manipulation of information in a nanomagnetic device *Nat. Nanotechnol.* **11** 437–43

[45] Winter J M 1961 Bloch Wall Excitation. Application to Nuclear Resonance in a Bloch Wall *Phys. Rev.* **124** 452–9

[46] Garcia-Sanchez F, Borys P, Soucaille R, Adam J-P, Stamps R L and Kim J-V 2015 Narrow Magnonic Waveguides Based on Domain Walls *Phys. Rev. Lett.* **114** 247206

[47] Henry Y, Stoeffler D, Kim J-V and Bailleul M 2019 Unidirectional spin-wave channeling along magnetic domain walls of Bloch type *Phys. Rev. B* **100** 024416

[48] Allenspach R, Stampanoni M and Bischof A 1990 Magnetic domains in thin epitaxial Co/Au(111) films *Phys. Rev. Lett.* **65** 3344

[49] Davies J E, Hellwig O, Fullerton E E, Denbeaux G, Kortright J B and Liu K 2004 Magnetization reversal of Co/Pt multilayers: Microscopic origin of high-field magnetic irreversibility *Phys. Rev. B - Condens. Matter Mater. Phys.* **70** 224434

[50] Thiele J U, Folks L, Toney M F and Weller D K 1998 Perpendicular magnetic anisotropy and magnetic domain structure in sputtered epitaxial FePt (001) L10 films *J. Appl. Phys.* **84** 5686

[51] Tacchi S, Fin S, Carlotti G, Gubbiotti G, Madami M, Barturen M, Marangolo M, Eddrief M, Bisero D, Rettori a. and Pini M G 2014 Rotatable magnetic anisotropy in a Fe 0.8 Ga 0.2 thin film with stripe domains: Dynamics versus statics *Phys. Rev. B - Condens. Matter Mater. Phys.* **89** 1–6

[52] Hierro-Rodriguez A, Vélez M, Morales R, Soriano N, Rodríguez-Rodríguez G, Álvarez-Prado L M, Martín J I and Alameda J M 2013 Controlled nucleation of topological defects in the stripe domain patterns of lateral multilayers with perpendicular magnetic anisotropy *Phys. Rev. B - Condens. Matter Mater. Phys.* **88** 174411

[53] Coïsson M, Barrera G, Celegato F and Tiberto P 2019 Rotatable magnetic anisotropy in Fe 78 Si 9 B 13 thin films displaying stripe domains *Appl. Surf. Sci.* **476** 402–11

[54] Wagner K, Kákay A, Schultheiss K, Henschke A, Sebastian T and Schultheiss H 2016 Magnetic domain walls as reconfigurable spin-wave nanochannels *Nat. Nanotechnol.* **11** 432–6

[55] Albisetti E, Petti D, Sala G, Silvani R, Tacchi S, Finizio S, Wintz S, Calò A, Zheng X, Raabe J, Riedo E and Bertacco R 2018 Nanoscale spin-wave circuits based on engineered reconfigurable spin-textures *Commun. Phys.* **1** 56

[56] Sluka V, Schneider T, Gallardo R A, Kákay A, Weigand M, Warnatz T, Mattheis R, Roldán-Molina A, Landeros P, Tiberkevich V, Slavin A, Schütz G, Erbe A, Deac A, Lindner J, Raabe J, Fassbender J and Wintz S 2019 Emission and propagation of 1D and 2D spin waves with nanoscale wavelengths in anisotropic spin textures *Nat. Nanotechnol.* **14** 328–33

[57] Yu H, Duerr G, Huber R, Bahr M, Schwarze T, Brandl F and Grundler D 2013 Omnidirectional spin-wave nanograting coupler *Nat. Commun.* **4** 2702

[58] Yu H, d' Allivy Kelly O, Cros V, Bernard R, Bortolotti P, Anane A, Brandl F, Heimbach F and Grundler D 2016 Approaching soft X-ray wavelengths in nanomagnet-based microwave technology *Nat. Commun.* **7** 11255

[59] Demidov V E, Urazhdin S and Demokritov S O 2010 Direct observation and mapping of spin waves emitted by spin-torque nano-oscillators *Nat. Mater.* **9** 984–8

[60] Madami M, Bonetti S, Consolo G, Tacchi S, Carlotti G, Gubbiotti G, Mancoff F B, Yar M a and Åkerman J 2011 Direct observation of a propagating spin wave induced by spin-transfer torque *Nat. Nanotechnol.* **6** 635–8

[61] Wintz S, Tiberkevich V, Weigand M, Raabe J, Lindner J, Erbe A, Slavin A and Fassbender J 2016 Magnetic vortex cores as tunable spin-wave emitters *Nat. Nanotechnol.* **11** 948–53

[62] Dieterle G, Förster J, Stoll H, Semisalova A S, Finizio S, Gangwar A, Weigand M, Noske M, Fähnle M, Bykova I, Gräfe J, Bozhko D A, Musiienko-Shmarova H Y, Tiberkevich V, Slavin A N, Back C H, Raabe J, Schütz G and Wintz S 2019 Coherent Excitation of Heterosymmetric Spin Waves with Ultrashort Wavelengths *Phys. Rev. Lett.* **122** 117202

[63] Mayr S, Flajsman L, Finizio S, Hrabec A, Weigand M, Förster J, Stoll H, Heyderman L J, Urbanek M, Wintz S and Raabe J 2021 Spin-wave emission from vortex cores under static magnetic bias fields *Nano Lett.* **21** 1584–90

[64] Hermsdoerfer S J, Schultheiss H, Rausch C, Schäfer S, Leven B, Kim S-K and Hillebrands B 2009 A spin-wave frequency doubler by domain wall oscillation *Appl. Phys. Lett.* **94** 223510

[65] Wiele B Van De, Hämäläinen S J, Bal P and Montoncello F 2016 Tunable short-wavelength spin wave excitation from pinned magnetic domain walls 1–11

[66] Hämäläinen S J, Brandl F, Franke K J A, Grundler D and van Dijken S 2017 Tunable Short-Wavelength Spin-Wave Emission and Confinement in Anisotropy-Modulated Multiferroic Heterostructures *Phys. Rev. Appl.* **8** 014020

[67] Holländer R B, Müller C, Schmalz J, Gerken M and McCord J 2018 Magnetic domain walls as broadband spin wave and elastic magnetisation wave emitters *Sci. Rep.* **8** 13871

[68] Grünberg P 1981 Magnetostatic spin-wave modes of a heterogeneous ferromagnetic double layer *J. Appl. Phys.* **52** 6824–9

[69] Bayer C, Schultheiss H, Hillebrands B and Stamps R L 2005 Phase shift of spin waves traveling through a 180° Bloch-domain wall *IEEE Trans. Magn.* **41** 3094–6

[70] Hertel R, Wulfhekel W and Kirschner J 2004 Domain-wall induced phase shifts in spin waves *Phys. Rev. Lett.* **93** 1–4

[71] Macke S and Goll D 2010 Transmission and reflection of spin waves in the presence of Néel walls *J. Phys. Conf. Ser.* **200** 042015

[72] Chang L-J, Liu Y-F, Kao M-Y, Tsai L-Z, Liang J-Z and Lee S-F 2018 Ferromagnetic domain walls as spin wave filters and the interplay between domain walls and spin waves *Sci. Rep.* **8** 3910

[73] Borys P, Garcia-Sanchez F, Kim J Von and Stamps R L 2016 Spin-Wave Eigenmodes of Dzyaloshinskii Domain Walls *Adv. Electron. Mater.* **2** 1500202

[74] Wang X G, Guo G H, Zhang G F, Nie Y Z and Xia Q L 2013 Spin-wave resonance reflection and spin-wave induced domain wall displacement *J. Appl. Phys.* **113** 213904

[75] Buijnsters F J, Ferreiros Y, Fasolino A and Katsnelson M I 2016 Chirality-Dependent Transmission of Spin Waves through Domain Walls *Phys. Rev. Lett.* **116** 147204

[76] Pirro P, Koyama T, Brächer T, Sebastian T, Leven B and Hillebrands B 2015 Experimental observation of the interaction of propagating spin waves with Néel domain walls in a Landau domain structure *Appl. Phys. Lett.* **106** 232405

[77] Wojewoda O, Hula T, Flajšman L, Vaňatka M, Gloss J, Holobrádek J, Staňo M, Stienen S, Körber L, Schultheiss K, Schmid M, Schultheiss H and Urbánek M 2020 Propagation of spin waves through a Néel domain wall *Appl. Phys. Lett.* **117** 3–8

[78] Hämäläinen S J, Madami M, Qin H, Gubbiotti G and van Dijken S 2018 Control of spin-wave transmission by a programmable domain wall *Nat. Commun.* **9** 4853

[79] Hioki T, Tsuboi R, Johansen T H, Hashimoto Y and Saitoh E 2020 Snell's law for spin waves at a 90°

magnetic domain wall *Appl. Phys. Lett.* **116**

[80] Li Z, Wang X, Wang D, Nie Y, Tang W and Guo G 2015 Reconfigurable magnonic crystal consisting of periodically distributed domain walls in a nanostrip *J. Magn. Magn. Mater.* **388** 10–5

[81] Wang X, Guo G, Li Z, Wang D, Nie Y and Tang W 2015 Spin-wave propagation in domain wall magnonic crystal *EPL (Europhysics Lett.* **109** 37008

[82] Camara I S, Tacchi S, Garnier L C, Eddrief M, Fortuna F, Carlotti G and Marangolo M 2017 Magnetization dynamics of weak stripe domains in Fe–N thin films: a multi-technique complementary approach *J. Phys. Condens. Matter* **29** 465803

[83] Garnier L C, Marangolo M, Eddrief M, Bisero D, Fin S, Casoli F, Pini M G, Rettori A and Tacchi S 2020 Stripe domains reorientation in ferromagnetic films with perpendicular magnetic anisotropy *J. Phys. Mater.* **3** 024001

[84] Fin S, Tomasello R, Bisero D, Marangolo M, Sacchi M, Popescu H, Eddrief M, Hepburn C, Finocchio G, Carpentieri M, Rettori A, Pini M G and Tacchi S 2015 In-plane rotation of magnetic stripe domains in Fe1-xGax thin films *Phys. Rev. B - Condens. Matter Mater. Phys.* **92** 224411

[85] Banerjee C, Gruszecki P, Klos J W, Hellwig O, Krawczyk M and Barman A 2017 Magnonic band structure in a Co/Pd stripe domain system investigated by Brillouin light scattering and micromagnetic simulations *Phys. Rev. B* **96** 024421

[86] Chumak A V., Serga A A and Hillebrands B 2017 Magnonic crystals for data processing *J. Phys. D. Appl. Phys.* **50** 244001

[87] Tacchi S, Gubbiotti G, Madami M and Carlotti G 2017 Brillouin light scattering studies of 2D magnonic crystals *J. Phys. Condens. Matter* **29** 073001

[88] Liu C, Wu S, Zhang J, Chen J, Ding J, Ma J, Zhang Y, Sun Y, Tu S, Wang H, Liu P, Li C, Jiang Y, Gao P, Yu D, Xiao J, Duine R, Wu M, Nan C-W, Zhang J and Yu H 2019 Current-controlled propagation of spin waves in antiparallel, coupled domains *Nat. Nanotechnol.* **14** 691–7

[89] Fert A, Reyren N and Cros V 2017 Magnetic skyrmions: Advances in physics and potential applications *Nat. Rev. Mater.* **2**

[90] Seki S, Garst M, Waizner J, Takagi R, Khanh N D, Okamura Y, Kondou K, Kagawa F, Otani Y and Tokura Y 2020 Propagation dynamics of spin excitations along skyrmion strings *Nat. Commun.* **11** 1–7

[91] Han J, Zhang P, Hou J T, Siddiqui S A and Liu L 2020 Erratum for the Report “Mutual control of coherent spin waves and magnetic domain walls in a magnonic device” by J. Han, P. Zhang, J. T. Hou, S. A. Siddiqui, L. Liu *Science (80-.).* **368** eabc1767

[92] Zhou Z wei, Wang X guang, Nie Y zhuang, Xia Q lin and Guo G hua 2021 Spin wave frequency comb generated through interaction between propagating spin wave and oscillating domain wall *J. Magn. Magn. Mater.* **534** 168046

[93] Qin H, Dreyer R, Woltersdorf G, Taniyama T and van Dijken S 2021 Electric-Field Control of Propagating Spin Waves by Ferroelectric Domain-Wall Motion in a Multiferroic Heterostructure *Adv. Mater.* **2100646** 2100646

[94] Chang L J, Chen J, Qu D, Tsai L Z, Liu Y F, Kao M Y, Liang J Z, Wu T S, Chuang T M, Yu H and Lee S F 2020

Spin Wave Injection and Propagation in a Magnetic Nanochannel from a Vortex Core *Nano Lett.* **20** 3140–6

[95] Li Z, Dong B, He Y, Chen A, Li X, Tian J H and Yan C 2021 Propagation of Spin Waves in a 2D Vortex Network *Nano Lett.*

[96] Lan J, Yu W and Xiao J 2017 Antiferromagnetic domain wall as spin wave polarizer and retarder *Nat. Commun.* **8** 1–7

[97] Yu W, Lan J and Xiao J 2020 Magnetic Logic Gate Based on Polarized Spin Waves *Phys. Rev. Appl.* **13** 1

[98] Datta S and Das B 1990 Electronic analog of the electro-optic modulator *Appl. Phys. Lett.* **56** 665–7

[99] Yu W, Lan J and Xiao J 2018 Polarization-selective spin wave driven domain-wall motion in antiferromagnets *Phys. Rev. B* **98** 1–7

[100] Xing X and Zhou Y 2016 Fiber optics for spin waves *NPG Asia Mater.* **8** e246-8

[101] Chen J, Hu J and Yu H 2020 Chiral Magnonics: Reprogrammable Nanoscale Spin Wave Networks Based on Chiral Domain Walls *iScience* **23** 101153

[102] Chen J, Yu T, Liu C, Liu T, Madami M, Shen K, Zhang J, Tu S, Alam M S, Xia K, Wu M, Gubbiotti G, Blanter Y M, Bauer G E W and Yu H 2019 Excitation of unidirectional exchange spin waves by a nanoscale magnetic grating *Phys. Rev. B* **100** 104427

[103] Lan J, Yu W, Wu R and Xiao J 2015 Spin-Wave Diode *Phys. Rev. X* **5** 1–7

[104] Zhang X, Liu T, Flatté M E and Tang H X 2014 Electric-field coupling to spin waves in a centrosymmetric ferrite *Phys. Rev. Lett.* **113** 1–5

[105] Wang X S R, Zhang H W and Wang X S R 2018 Topological Magnonics: A Paradigm for Spin-Wave Manipulation and Device Design *Phys. Rev. Appl.* **9** 24029

[106] Zhang L, Ren J, Wang J S and Li B 2013 Topological magnon insulator in insulating ferromagnet *Phys. Rev. B - Condens. Matter Mater. Phys.* **87** 144101

[107] Shindou R, Ohe J I, Matsumoto R, Murakami S and Saitoh E 2013 Chiral spin-wave edge modes in dipolar magnetic thin films *Phys. Rev. B - Condens. Matter Mater. Phys.* **87** 174402

[108] Nakane R, Tanaka G and Hirose A 2018 Reservoir Computing with Spin Waves Excited in a Garnet Film *IEEE Access* **6** 4462–9

[109] Papp Á, Porod W and Csaba G 2021 Nanoscale neural network using non-linear spin-wave interference *Nat. Commun. 2021 121* **12** 1–8

[110] Wang Q, Chumak A V. and Pirro P 2021 Inverse-design magnonic devices *Nat. Commun. 2021 121* **12** 1–9